Journal of Water Process Engineering 60 (2024) 105185

Contents lists available at ScienceDirect

Journal of Water Process Engineering

journal homepage: www.elsevier.com/locate/jwpe

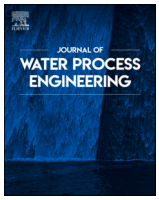

Evaluation of the performance of Fe_3O_4-NPs/PVDF nanocomposite membrane for removal of BTEX from contaminated water

Ngozi Enemuo [a], Heidi Richards [a], Michael O. Daramola [b,*]

[a] Molecular Sciences Institute, School of Chemistry, University of the Witwatersrand, Private Bag X3, WITS, 2050 Johannesburg, South Africa
[b] Sustainable Energy and Environment Research Group (SEERG), Department of Chemical Engineering, Faculty of Engineering, Built Environment and Information Technology, University of Pretoria, Hatfield, 0028 Pretoria, South Africa

ARTICLE INFO

Editor: ChoeEarn Choong

Keywords:
PVDF membrane
Biogenically-synthesized Fe_3O_4-NPs
BTEX
Hydrophilic
Water treatment

ABSTRACT

With the increase in reported cases of toxic organic contaminants such as benzene, toluene, ethylbenzene, and xylene (BTEX) in the aquatic environment, membrane technology offers a viable option for removing BTEX from wastewater. However, hydrophilic modification of the membranes is vital to reduce the rapid accumulation of the BTEX organic contaminants and maintain improved membrane performance in BTEX removal. In this study, biogenically-synthesized Fe_3O_4-NPs were embedded into a PVDF membrane to endow the membrane with hydrophilicity, which necessitates the reduction in BTEX accumulation on the membrane, consequently maintaining improved membrane performance towards BTEX removal. Different Fe_3O_4-NPs loadings (0 wt% to 5 wt %) were used for the PVDF modification to establish the optimum blending amount of the Fe_3O_4-NPs required to achieve the most effective membrane. The water contact angle was reduced from 84.2° (pristine PVDF) to 52° for the membrane modified with 1 wt% of the Fe_3O_4-NPs. Other membrane features such as porosity, surface roughness, and mechanical strength were also enhanced. Performance evaluation of the membranes revealed that the flux and BTEX rejection of the Fe_3O_4-NPs/PVDF membrane were improved. The antifouling test results showed a reduction in the total fouling from 52.1 % (pristine membrane) to 36.3 % for the membrane modified with 1 wt% of the Fe_3O_4-NPs. Our findings provide a strategy utilizing biogenically synthesized Fe_3O_4-NPs to enhance PVDF membranes' performance for removing BTEX from wastewater.

1. Introduction

Discharging untreated or poorly treated wastewater into water bodies is a global challenge that has highlighted the need for continuous development of better means of wastewater treatment before discharge [1–3]. One of the implications of discharging poorly treated wastewater into the water sources is the release of harmful contaminants into our aquatic system [4,5]. Among the top contaminants reported to be released into the water bodies from industrial discharge are benzene, toluene, ethylbenzene, and xylene, collectively known as BTEX [6–8]. According to the USEPA [9], the health implications of exposure to BTEX-contaminated water include cancer, reproductive complications, and neurological problems, among others. BTEX also poses environmental issues such as the pollution of aquatic systems, and its volatilization from the contaminated water body into the atmosphere causes poor air quality [10,11].

In response to the adverse health and environmental consequences of BTEX-contaminated water bodies, several treatment techniques have been developed to ensure the removal of BTEX from wastewater before discharge. Such treatment methods include hydrocyclones, flotation, API separators, and membrane technology [12–14]. Among these treatment techniques, membrane technology is the most efficient and effective. In contrast, the other techniques are either not very effective in removing BTEX, are cost and energy-intensive, or lead to secondary pollution.[15,16]. Although most membranes, such as polyvinylidene fluoride (PVDF), possess the ideal physical properties required for BTEX wastewater treatment, they are limited by their hydrophobic nature [17]. This limitation springs from the strong hydrophobic interaction between the membrane and the BTEX organic contaminants, which results in rapid accumulation of the BTEX on the membrane and subsequent membrane fouling [18]. Membrane fouling results in deterioration of the membrane performance, such as flux decline, poor rejection, and reduced membrane lifespan [19–21]. To minimize membrane fouling and maintain good membrane performance during

* Corresponding author.
E-mail address: michael.daramola@up.ac.za (M.O. Daramola).

https://doi.org/10.1016/j.jwpe.2024.105185
Received 9 November 2023; Received in revised form 8 March 2024; Accepted 17 March 2024
Available online 25 March 2024

the treatment of organic contaminated wastewater, the membrane is made hydrophilic by incorporating hydrophilic components such as hydrophilic polymers and nanoparticles (NPs) into the membrane [22–24]. The incorporated hydrophilic components not only improve the membrane's performance but also reinforce the membrane's physical properties, such as morphology and mechanical stability [25–27].

Over the years, nanoparticles such as TiO_2 [28], Ag [29], Al_2O_3 [30], and Fe_3O_4 [31] have successfully been utilized in enhancing the hydrophilicity of membranes to reduce fouling and achieve good membrane performance in the removal of organic contaminants from wastewater. Matindi et al. [32] incorporated TiO_2 NPs into a polyethersulfone/polysulfone (PES/PS) composite membrane to improve the membrane performance in oil-in-water emulsion separation. They reported that the embedded TiO_2 significantly improved the hydrophilicity of the membrane; as a consequence, the membrane performance, such as flux and separation efficiency, was enhanced. In another modification strategy, Fe_3O_4@MoS_2 NPs were anchored in a PES membrane, and its performance integrity in treating bovine serum albumin (BSA) and humic acid (HA) contaminated water was assessed [33]. The Fe_3O_4@MoS_2 NPs modified membrane improved its permeability and rejection due to the enhanced hydrophilicity introduced in the membrane by the Fe_3O_4@MoS_2 NPs [33]. The removal efficiency of another organic contaminant, methylene blue, was improved by modifying the PVDF membrane used for the removal of the dye with Fe_3O_4 NPs [34].

Very little research has been reported on treating BTEX-contaminated wastewater using Fe_3O_4 NPs-modified membrane. In fact, to the best of our knowledge, only two research studies have been conducted on iron or iron oxide-modified membranes for the treatment of BTEX-contaminated wastewater. The first research incorporated Fe-NPs into a polyethersulfone (PES) membrane for the treatment of BTEX-contaminated water and reported an improvement in the performance of the modified membrane compared to the pristine PES [35]. However, the Fe-NPs used in the fabrication were reported to be agglomerated, and the cumulative BTEX rejection of the modified membrane was 64.55 % [35]. The second research used a tannin iron complex (TA-Fe^{III}), not iron nanoparticles, to modify a PES membrane to treat BTEX wastewater, and enhanced performance of the modified membrane was reported [36].

Considering the studies mentioned above on the use of iron-modified membranes for the treatment of BTEX-contaminated wastewater, there is a need to improve the dispersion of the iron nanoparticles during their synthesis. This is because the incorporation of agglomerated nanoparticles in a membrane often adversely affects the physical and performance characteristics of the membrane [37–40]. To establish the optimum conditions for treating the BTEX-contaminated wastewater, there is also a need to explore the influence of the operational conditions on the performance of the modified membrane. In addition, an antifouling test on the iron-modified membrane is needed to establish the effect of the incorporated NPs on fouling mitigation. Furthermore, PVDF is known to be more chemically resistant to all four components of BTEX: benzene, toluene, ethylbenzene, and xylene [41]. Hence, using a more BTEX-resistant base polymer to treat the wastewater would ensure that there would be no or minimal deterioration of the membrane performance due to chemical degradation of the polymer by the BTEX contaminants.

Therefore, in this study, biogenic synthesis of Fe_3O_4-NPs was performed using the extract of pomegranate leaf to reduce iron precursor to the Fe_3O_4-NPs, and the leaf extract also stabilized the synthesized Fe_3O_4-NPs; thus, a dispersed NPs was obtained. Subsequently, the PVDF membrane was modified with the biogenically synthesized Fe_3O_4-NPs, and the effect of the NPs on the physical features and performance of the membrane was investigated. Furthermore, the effect of pressure and BTEX feed concentration on the flux and rejection of the Fe_3O_4-NPs/PVDF membrane was also investigated. In addition, the influence of the Fe_3O_4-NPs on the antifouling tendency of the modified membrane was further assessed.

2. Experimental

2.1. Materials

PVDF pellets (M_w ~ 180,000gmol^{-1}), PSF pellets (M_w ~ 35,000gmol^{-1}), 1-methyl-2-pyrrolidinone (NMP, ≥99.0 %), iron (III) chloride ($FeCl_3$), benzene (99.8 %), toluene (99.9 %), ethylbenzene (>99.9 %), and xylene (≥99 %) were purchased from Sigma Aldrich. The Direct-Q UV millipore system supplied deionized water (DI water, 18.2 MΩcm @25oC). All the reagents were used as received without any further purification. The pomegranate leaves were collected from the tree at the School of Chemical Engineering, University of the Witwatersrand, Johannesburg.

2.2. Synthesis of Fe_3O_4-NPs

The Fe_3O_4-NPs were biogenically synthesized using the extract of the pomegranate leaves. To obtain the leaves extract, pomegranate leaves were thoroughly washed with water to remove dust particles, dried, and then ground with a grinder. 20 g of the dried leaves powder was mixed with 200 mL of DI water and shaken for 8 h at 150 rpm, followed by sonication for 30 min. The mixture was first filtered with a sieve and then with Whatman grade 1 filter paper. The obtained filtrate was stored at 4 °C for the synthesis of the Fe_3O_4-NPs.

To synthesize the Fe_3O_4-NPs, $FeCl_3$ was biogenically reduced by the leaves extract following a method by Xu et al. [42] with some modifications, which include changing the reaction duration and temperature. Plant extracts are known to exhibit an inherent ability to act as reducing, size-control, and stabilizing agents in the synthesis of nanoparticles [43]. For this synthesis, 1.2 g of $FeCl_3$ was thoroughly dissolved in 70 mL of DI water, and 140 mL of leaf extract was added to the $FeCl_3$ solution under rigorous stirring. The reaction mixture was continuously stirred for 3 h at 80 °C, and during this time, the colour of the reaction solution changed from yellow ($FeCl_3$ solution) to black, indicating the formation of the Fe_3O_4-NPs. The resulting mixture was centrifuged, and the product was washed three times with ethanol and water to remove impurities and then dried in an oven for 3 h at 50 °C to obtain the Fe_3O_4-NPs in dry form for the enhancement of the features of PVDF membranes for BTEX wastewater treatment.

2.3. Fabrication of Fe_3O_4-NPs/PVDF membranes

The base membrane ideal for the BTEX wastewater treatment was selected based on the ability of the membrane to exhibit high tolerance to BTEX water with no or minimal membrane damage. Two fabricated membranes (PSF and PVDF) were tested for their tolerance towards BTEX water by immersing the membranes in different concentrations (500 ppm, 1000 ppm, and 2000 ppm) of BTEX solutions at room temperature for 30 days. The exposed membranes were removed from the BTEX solutions after 30 days, rinsed with DI water, and oven-dried at 40 °C for 2 h. Physical observation and SEM were used to determine the BTEX tolerance of the two membranes. The membrane with the best tolerance to BTEX was subsequently chosen as the base membrane for treating the BTEX wastewater.

PVDF was selected as the base membrane based on its high tolerance to BTEX water, as shown in the results session in Figs. 4 and 5. Various amounts of the Fe_3O_4-NPs, ranging from 0.0 to 5.0 wt% loadings, as depicted in Table 2, were embedded in the PVDF membrane. The Fe_3O_4-NPs/PVDF membranes were prepared by thoroughly dispersing the appropriate amount of the Fe_3O_4-NPs in NMP and dissolving the PVDF pellets in a separate NMP solvent. Well-dispersion of the Fe_3O_4-NPs was achieved by stirring the Fe_3O_4-NPs suspension for 2 h, followed by sonication for 30 mins. The Fe_3O_4-NPs suspension was then slowly poured into the PVDF solution under constant stirring, and the mixture

was stirred for 8 h at 50 °C. Then, the obtained dope solution was left to degas for 1 h to remove air bubbles and cast on an elcometer film applicator. The cast membranes were fabricated using the non-solvent induced phase inversion method with DI water as the coagulation bath. The fabricated membranes were washed with DI water to remove any remaining solvent and dried in the oven at 40 °C for 6 h.

2.4. Characterization of the leaf extract, Fe_3O_4-NPs, and the membranes

The leaf extract was analyzed to determine its constituent phytochemicals using an Agilent GC 7890B equipped with a 30 m × 0.25 mm ID × 0.25 μm Rxi-5Sil MS capillary column. The instrument is also equipped with a Gerstel multipurpose sampler and a Pegasus 4D GC × GC-TOFMS. Before the analysis, the leaves extract was filtered using a 0.45 μm PTFE filter. The injection volume was 1 μL in a splitless mode, and helium was the carrier gas. The oven temperature gradient was programmed as follows: 50 °C for 30 s, then 300 °C for 2 min at a rate of 15 °C/min.

The Fe_3O_4-NPs were identified via the X-ray diffraction (XRD) using Bruker D2 phaser, and the functional groups were evaluated using Fourier transform infrared spectroscopy (FTIR) performed on a Bruker Tensor 27. The textural property of the Fe_3O_4-NPs was determined via N_2 physisorption at 77 k using Brunauer-Emmett-Teller (BET) Micrometrics Tristar Plus 3.03. The morphology of the Fe_3O_4-NPs was studied using a high-resolution Carl Zeiss scanning electron microscopy (SEM) and FEI Tecnai T12 transmission electron microscopy (TEM). Energy-dispersive X-ray spectroscopy (EDX) was done using the same Carl Zeiss SEM. For X-ray photoelectron spectroscopy (XPS) measurements, X-rays were generated from a monochromatic Al K_a X-ray source. A hemispherical electron energy analyzer, SPECS Phoibos 150, determined the energies of the emitted electrons. The total energy resolution was approximately 0.7 eV.

The morphology of the fabricated membranes was obtained using a high-resolution Carl Zeiss SEM and the surface roughness of the membranes was checked with WITec alpha 300 atomic force microscope (AFM). The contact angle was measured by the sessile drop method using a KRUSS G10 goniometer. Seven measurements were done for each membrane, and the average was calculated. The thickness of the prepared membranes (excluding the membranes used for the BTEX tolerance test) was measured using a digital micrometer. The thickness of each of the membranes was measured at five different positions, and the average thickness was calculated. ImageJ open-source software was used to measure the pore size of the membrane from the SEM images, and the mean pore size was calculated. The porosity (ε) and equilibrium water content (EWC) of the membranes were measured using the gravimetric method according to Eq. (1) and Eq. (2), respectively.

$$\varepsilon\ (\%) = \frac{(W_{wet} - W_{dry})}{\rho \times A \times l} \times 100 \tag{1}$$

$$EWC\ (\%) = \left(\frac{W_{wet} - W_{dry}}{W_{wet}}\right) \times 100 \tag{2}$$

where W_{dry} and W_{wet} represent the masses of the dry membrane and the wet membrane respectively. $\rho, A,$ and l are the density of water (g/cm^3), the effective area of the tested membrane (m^2), and the thickness of the membrane (m), respectively. The wet membrane was obtained by immersing the membrane in DI water for 48 h. After 48 h, the membrane was removed from the DI water, thoroughly wiped to remove excess water on the membrane, and subsequently weighed to obtain its weight.

The surface charge properties of the membranes were obtained using the Zetasizer Nano ZS system, Malvern Instruments. Each membrane was soaked in KOH (0.01 M, 300 mL) electrolyte solution for 48 h, and measurements were conducted at pH ranging from 1.8 to 12.1 at 25 °C. The membrane was cut and then fitted with the active side facing upward into the custom dip-cell immersed in the background electrolyte solution. The pH was adjusted using a dilute HCl and NaOH solution. A thermogravimetric analyzer, TA SDT Q600, was used to measure the thermal stability of the membranes between 25 °C and 700 °C at a heating rate of 10 °C/min under nitrogen. The mechanical properties were determined using a Tesla analyzer, XT plus TA.

2.5. Membrane performance evaluation

For the performance evaluation, a dead-end stirred cell (HP4750; Sterlitech Corp., USA) was utilized for the filtration of DI water and synthetic BTEX water. Synthetic BTEX water was used because of the difficulty in accessing BTEX-contaminated wastewater from the industries. The pressure at which filtration is performed has an impact on the membrane flux and rejection [82]. Hence, the investigation of the effect of pressure on the membrane flux and rejection gives an indication of the ideal pressure required to achieve good flux and rejection. To measure the effect of pressure on the pure water flux of the membranes, each membrane was mounted on the filtration cell, and the cell was filled with DI water. The DI water was filtered through the membrane for 1 h at pressures of 100 kPa, 300 kPa, and 500 kPa, and the permeate was collected and measured. Each membrane was compacted using DI water to achieve a steady permeation before filtration. The pure water flux J_w (L m^{-2} h^{-1}) was calculated using Eq. (3), where V is the volume of the permeate (L), A is the effective membrane area (m^2), and t is the permeation time (min) [44].

$$J_w = \frac{V}{A \times t} \tag{3}$$

The effect of pressure on the BTEX flux and rejection of the membranes was measured by filtering synthetic BTEX water containing 100 ppm each of benzene, toluene, ethylbenzene, and xylene through the individual membranes under continuous stirring at a pressure of 100 kPa, 300 kPa, and 500 kPa using the same procedure described above. The BTEX flux was also calculated using Eq. (3), while the BTEX rejection was calculated according to Eq. (4).

$$R\ (\%) = \frac{C_f - C_p}{C_f} \tag{4}$$

where C_f is the BTEX concentration in the prepared feed water (ppm), and C_p is the BTEX concentration in the permeate (ppm). C_p was measured using an Agilent 7890A gas chromatograph GC, with a 30 m × 0.25 mm ID BP5MS × 0.25 μm column, and equipped with an Agilent 7693A automatic liquid sampler and a flame ionization detector FID. The injection volume was 0.2 μL in splitless mode, and the carrier gas was nitrogen set at a constant flow rate of 2.64 mL/min. The oven initial temperature was set at 40 °C and held for 2 min, then ramped to 90 °C at 10 °C/min, held for 3 min, and finally to 200 °C at a rate of 20 °C/min and held for 2 min.

The concentration of feed solutions also affects the rejection capacity of membranes [45]; hence, the BTEX rejection percentage of the membranes was evaluated at feed concentrations of 50, 100, 150, and 200 ppm to establish the feed concentrations that are ideal for effective BTEX rejection using the fabricated membranes.

The fouling resistance of the membranes towards BTEX was assessed by measuring four parameters: reversible fouling ratio (R_r), irreversible fouling ratio (R_{ir}), flux recovery ratio (FRR), and total fouling ratio (R_t). Antifouling test was done by first performing pure water filtration for 1 h, followed by BTEX filtration (500 mL of 100 ppm) under continuous stirring, then cleaning the membranes with water through backwashing followed by mild sonication in water. The backwashing of the membrane was performed by placing the bottom side of the membrane in an upward position in the dead-end cell and filtering 200 mL of DI water through the membrane. This was followed by another filtration of 100 mL of DI water through the top side of the membrane and subsequent mild sonication of the membrane in DI water for 15 min. The cleaned membrane was again used for water filtration. The equations for

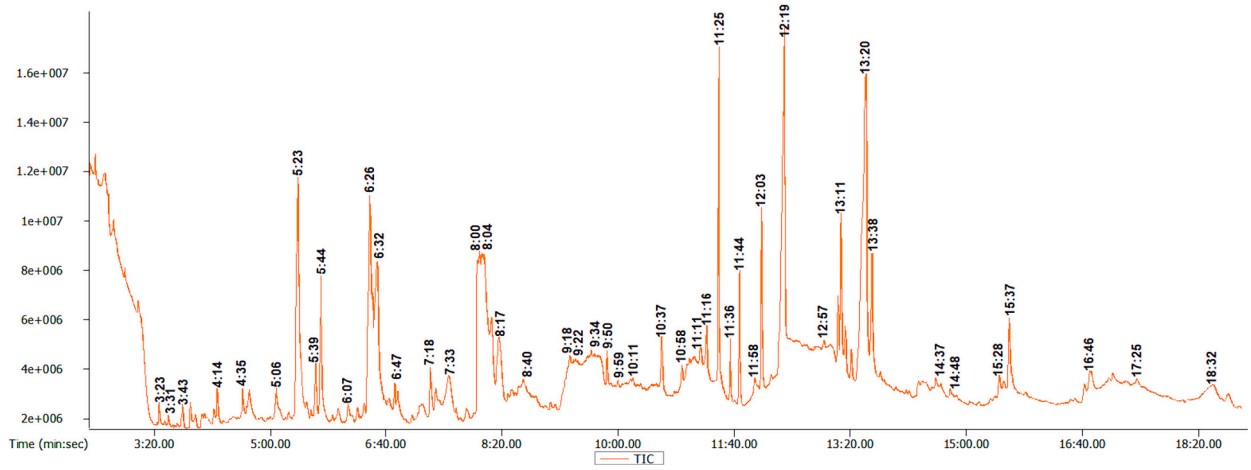

Fig. 1. GC–MS chromatogram of the pomegranate leaves extract.

calculating the R_r, R_{ir}, FRR, and R_t are shown in Eq. (5), Eq. (6), Eq. (7), and Eq. (8), respectively.

$$R_r(\%) = \left(\frac{J_C - J_{BTEX}}{J_w}\right) \times 100 \quad (5)$$

$$R_{ir}(\%) = \left(\frac{J_w - J_c}{J_w}\right) \times 100 \quad (6)$$

$$FRR\ (\%) = \left(\frac{J_c}{J_w}\right) \times 100 \quad (7)$$

$$R_t = \left(\frac{J_w - J_{BTEX}}{J_w}\right) \times 100 \quad (8)$$

Where J_w is the pure water flux, J_{BTEX} is the flux of the BTEX solution, and J_c is the flux of the cleaned membranes.

3. Results and discussion

3.1. Phytochemical composition of the pomegranate leaf extract and characterization of the biosynthesized Fe_3O_4-NPs

The phytochemical composition of the leaf extract of the pomegranate was determined using GC–MS, and the chromatogram is shown in Fig. 1. The GC–MS chromatogram indicates the presence of many active phytochemicals such as 2,3-Dihydroxy-2-methylpentanoic acid, 2-Propenoic acid, 3-(2-furanyl)-, Phenol, 4-nitro-, and 2-Methoxy-4-vinylphenol in the leaf extract. These phytochemicals are the active compounds capable of bio-reducing metal precursors and subsequently stabilizing the biogenically produced nanoparticles [46]; hence they are responsible for the bio-reduction of the iron precursor to the Fe_3O_4-NPs and stabilizing the NPs. Table 1 presents some of the active compounds with their retention time (R_T), molecular weight, and structural formula. The other active compounds assigned in the GC–MS chromatogram are presented in Table S1.

The XRD pattern of the Fe_3O_4-NPs shown in Fig. 2(a) reveals the characteristic peaks at $2\theta = 30.1°$, 35.5°, 43.1°, 53.4°, 57.0°, and 62.6° corresponding to diffraction planes of (220), (311), (400), (422), (511), and (440), respectively, indicating that the synthesized NPs are Fe_3O_4 [47]. The observed sharp peaks confirm the ability of the leaves extract of the pomegranate to completely reduce the iron (III) chloride precursor to crystalline Fe_3O_4-NPs.

FTIR study was performed to identify and compare the functional groups present in the leaves extract, and the Fe_3O_4-NPs to establish the capping ability of the leaves extract on the Fe_3O_4-NPs. As shown in the FTIR spectra depicted in Fig. 2(b), a broad peak at about 3320 cm^{-1} is seen for both the leaves extract and the Fe_3O_4-NPs and this peak corresponds to the O—H of hydroxyl-containing groups such as carboxylic acid, phenolic acids, alcohols, and phenols [48]. The pomegranate leaves are rich in such hydroxyl-containing compounds, which are deposited on the Fe_3O_4-NPs during the biogenic reduction of the iron precursor by the leaf extracts [49]. Other peaks at 1712 cm^{-1}, 1605 cm^{-1}, 1340 cm^{-1}, and 1069 cm^{-1}, which correspond to the C═O, C═C, O—H, and C—O groups, are seen in the spectra of the leaves extract and Fe_3O_4-NPs with a relative shift in the peak positions and intensity. This indicates the involvement of the various functional groups in the formation and capping of the Fe_3O_4-NPs [50].

The SEM and TEM images of the Fe_3O_4-NPs are depicted in Fig. 2(c) and 2(d), respectively, and describe the morphology of the NPs. As seen in the SEM image, the NPs were spherically shaped with nanoscale dimensions, with the smallest NPs being about 15 nm, as shown in the TEM image. Strong EDX signals (depicted in the inset of the SEM image) of elemental iron and oxygen confirm the presence of Fe_3O_4-NPs.

The textural property of the Fe_3O_4-NPs is presented in Fig. 2(e). The nitrogen adsorption/desorption isotherm curves obtained for the Fe_3O_4-NPs using the BET technique show a type IV adsorption-desorption isotherm, a characteristic feature of mesoporous materials [51]. Thus, the mesoporous nature of the Fe_3O_4-NPs could contribute to improving the flux of the membrane due to their characteristic uniform array of nanochannels that could facilitate the permeability of water through the membrane. In addition, the NPs have a high specific surface area of 81.95 m^2/g, which could necessitate the availability of the hydrophilic sites of the NPs, resulting in an enhanced contribution of the NPs to improve the membrane properties and performance. The desorption branch of the Barrett-Joyner-Halenda (BJH) method was used to determine the pore size distribution of the Fe_3O_4-NPs, and it shows that the Fe_3O_4-NPs have broad pore size distribution with an average pore size of 12.08 nm, as depicted in the inset in Fig. 2(e). However, most Fe_3O_4-NPs have small pore sizes within 1.73 nm and 20.64 nm.

The XPS spectrum of the Fe 2p core level is shown in Fig. 3. As is usual for fitting when Fe(III) components are involved, only the Fe $2p_{3/2}$ component was fitted [52]. A Shirley background was used. As can be seen, a good fit is obtained using the multiplets of Fe^{3+} and Fe^{2+} as calculated for Fe_3O_4 [52]. The differences in energies between the various peaks of the multiplets and their relative intensities were kept constant for the fit. This confirms that the iron present in the sample is Fe_3O_4. This can also be seen qualitatively from the line shape by comparison with the literature [53,54].

3.2. Characterization of Fe_3O_4-NPs/PVDF membrane

The outcome of the exposure of two polymeric membrane materials,

Table 1
Some of the active phytochemicals in the pomegranate leaves extract with their compound name, retention time (R_T), and structure.

Name of compound	R_T (min)	Molecular weight	Structural formula
2(5H)-Furanone	3:23	84	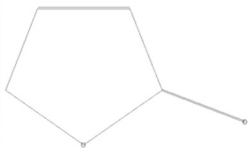
2,3-Dihydroxy-2-methylpentanoic acid	3:43	148	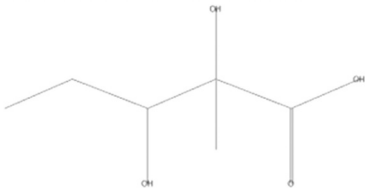
Formic acid, 2-methoxyphenyl ester	5:06	152	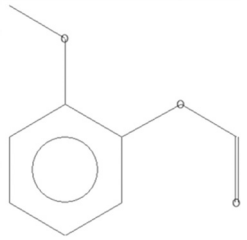
á-D-Glucopyranose pentaacetate	5:39	390	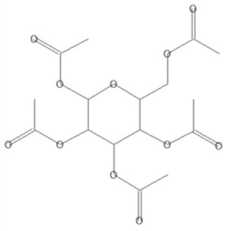
5-Hydroxymethylfurfural	6:32	126	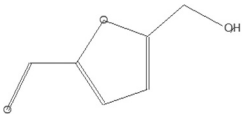
2-Methoxy-4-vinylphenol	7:18	150	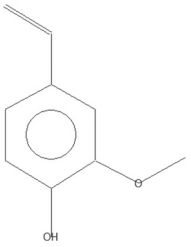
Isosorbide	8:00	146	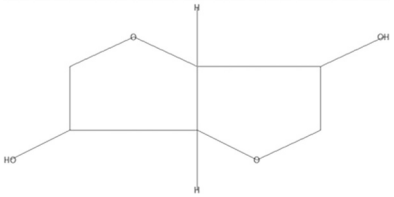
Glucuronamide	8:04	193	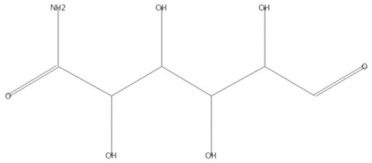

(*continued on next page*)

Table 1 (*continued*)

Name of compound	R_T (min)	Molecular weight	Structural formula
Rhamnose	8:17	164	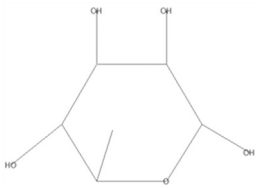
Phenol, 4-nitro-	9:22	134	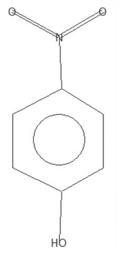
2-Cyclohexen-1-one, 4-(3-hydroxybutyl)-3,5,5-trimethyl-	10:37	210	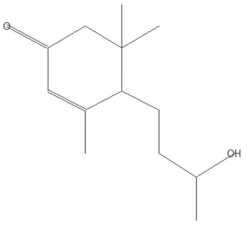
2-Propenoic acid, 3-(2-furanyl)-	12:11	138	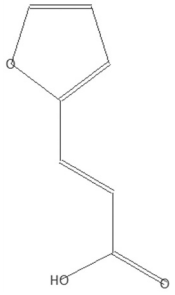

Table 2
Composition of the fabricated membranes.

Membrane ID	PVDF (wt%)	NMP (wt%)	Fe_3O_4-NPs (wt%)
PVDF 0	15	85.00	0.00
PVDF 0.05	15	84.95	0.05
PVDF 0.1	15	84.90	0.10
PVDF 0.2	15	84.80	0.20
PVDF 0.5	15	84.50	0.50
PVDF 1.0	15	84.00	1.00
PVDF 2.0	15	83.00	2.00
PVDF 3.0	15	82.00	3.00
PVDF 5.0	15	80.00	5.00

PSF and PVDF, to different concentrations of synthetic BTEX is shown in Figs. 4 and 5. Fig. 4 shows the membranes after exposure to the BTEX solution. The images show that the PSF was very prone to severe damage when exposed to BTEX. Hence, using PSF as a base membrane for BTEX wastewater treatment will result in rapid membrane damage by the BTEX contaminant, eventually leading to loss of membrane property and performance. In contrast, the PVDF membrane exhibited high tolerance to the BTEX solution under all the tested BTEX concentrations. The same observation was seen in the SEM images of the PSF and PVDF membranes depicted in Fig. 5. The SEM image shows that the morphology of the PSF membrane was severely affected as its finger-like pores were shrunk and damaged. In contrast, the morphology of the PVDF membrane was not affected by the BTEX exposure. Because of the excellent tolerance of the PVDF membrane to the target contaminant, it was selected as the base membrane in this study.

The results of the tests on four of the prepared membranes, PVDF 0, PVDF 0.2, PVDF 1.0, and PVDF 3.0, are mainly discussed for a comprehensible presentation of the findings of this study.

The chemical composition of the membranes was evaluated using FTIR, and the spectra are presented in Fig. 6. From the region of 600 cm^{-1} to 1500 cm^{-1}, no notable peak change was observed for both the pristine membrane and the modified membranes, and the peaks appearing in those regions are characteristic peaks for PVDF [55]. Two distinct peaks at 1650 cm^{-1} and 3400 cm^{-1} for C═O and OH stretching vibrations were observed for PVDF 1.0 and PVDF 3.0 membranes. These two peaks revealed the presence of carboxylic acid and hydroxyl groups in the embedded Fe_3O_4-NPs, which could be from chemical groups such as phenolic acid and phenol in the leaves extract of the pomegranate. The lack of notable presence of these two peaks in PVDF 0.2 could be due to the small amount of the Fe_3O_4-NPs incorporated into the membrane.

The SEM images of the membranes depicting their morphology are shown in Fig. 7. All the membranes have finger-like pore structures, which is indicative of membranes fabricated through nonsolvent-induced phase inversion [56,57]. The finger-like structures of the Fe_3O_4-NPs/PVDF membranes are broader and longer than that of the pristine membrane due to the hydrophilicity of the Fe_3O_4-NPs, which

Table 3
The thickness, porosity, EWC, and mean pore size of all the fabricated membranes.

Membrane ID	Thickness (μm)	Porosity (%)	EWC (%)	Mean pore size (nm)
PVDF 0	112 ± 4	60.5 ± 0.7	53.5 ± 0.7	40.3 ± 1.5
PVDF 0.05	110 ± 2	64.0 ± 0.8	60.5 ± 0.5	41.0 ± 1.7
PVDF 0.1	114 ± 2	67.0 ± 1.4	66.5 ± 0.7	44.0 ± 3.8
PVDF 0.2	109 ± 3	73.0 ± 1.4	70.5 ± 0.7	44.6 ± 3.2
PVDF 0.5	112 ± 3	75.0 ± 1.4	73.0 ± 1.4	48.3 ± 2.5
PVDF 1.0	109 ± 1	77.5 ± 0.7	75.5 ± 0.7	55.2 ± 0.9
PVDF 2.0	113 ± 3	73.5 ± 0.7	69.0 ± 1.4	54.6 ± 2.4
PVDF 3.0	112 ± 3	66.5 ± 1.1	65.5 ± 1.4	49.3 ± 1.5
PVDF 5.0	115 ± 1	62.0 ± 1.4	60.0 ± 0.8	42.3 ± 2.3

induces fast solvent and nonsolvent exchange during the phase inversion process [58,59]. Such well-formed finger-like macrovoids in the modified membranes are beneficial in improving the permeability of the membranes [60]. The dispersion of the Fe_3O_4-NPs on the surface and inner structure of the membranes are shown in the EDX mapping and higher magnification cross-section images, respectively. The EDX mapping shows fairly good dispersion of the Fe_3O_4-NPs in PVDF 0.2 and PVDF 1.0 membranes, while the Fe_3O_4-NPs in PVDF 3.0 seem more agglomerated. This correlates with the dispersion of the Fe_3O_4-NPs in the membranes' inner structure, which shows the agglomerated Fe_3O_4-NPs in the PVDF 3.0 membrane clogging its inner pores. Such NPs agglomeration often adversely affects the membrane property and performance [61].

The morphology of the membranes in terms of their surface roughness is presented in the AFM images in Fig. 8. An increment in the membranes' roughness was observed as the amount of the Fe_3O_4-NPs in the membrane increased, with the pristine PVDF membrane having the lowest surface roughness. The roughness parameter was obtained by measuring the membrane's average roughness (Sa) and root mean square (Sq). PVDF 0 has Sa and Sq values of 44.2 nm and 48.6 nm, respectively. The Sa and Sq values increased to 47.5 nm and 49.2 nm for PVDF 0.2, while the Sa and Sq values for PVDF 1.0 were 55.6 nm and 60.4 nm, respectively. However, the Sa and Sq values of PVDF 3.0, which were 45.8 nm and 48.9 nm, were lower than that of PVDF 0.2 and PVDF 1.0 but slightly higher than the roughness parameters of the pristine membrane. This deviation from the incremental trend observed in the modified membranes could be due to a decline in the porosity of PVDF 3.0 as well as the increased viscosity of the dope solution of PVDF 3.0, which led to the formation of a dense and smoother top layer [62]. A similar trend was obtained by Rowley and Abu-Zahra [63].

Fig. 9 (a) depicts the water contact angle of the membranes, which is a measure of their hydrophilicity. Hydrophilicity is a significant factor that determines the permeability and antifouling ability of membranes [24], and contact angle (CA) measurement offers a precise determination of hydrophilicity, with a lower contact angle signifying a hydrophilic membrane and vice versa [64]. As shown in Fig. 9(a), the pristine PVDF has a high CA of 84.2°, and a significant reduction in the CA of the membranes was seen with loading of the Fe_3O_4-NPs up to 1.0 wt%. Two fundamental properties of the NPs facilitate the improvement in hydrophilicity. First, the presence of the hydrophilic O—H functional group on the surface of the Fe_3O_4-NPs, as confirmed by the FTIR result, provided polar sites that can form hydrogen bonding with water, thereby enhancing the hydrophilicity of the membranes. Secondly, the inorganic nanoparticles, Fe_3O_4-NPs, are intrinsically hydrophilic,

Table 4
Comparison of the performance of the Fe_3O_4-NPs/PVDF membrane with other studies in the literature.

Membrane composition	PWF (L/m^{2}h)	%R	FRR	Ref.
TA-Fe^{III}/PES	150.0	≈ 90 %	–	[36]
Fe-NPs/ PES	84.73	≈ 60 %	–	[35]
Carbon nanotube/PVDF	7.1	≈ 90 %	–	[78]
Fe_3O_4-NPs/PVDF	266.0	≈ 80 %	≈ 80 %	This study

providing hydration sites on the membranes and thus contributing to their improved hydrophilicity [40,65]. At Fe_3O_4-NPs loadings above 1.0 wt%, agglomeration, a characteristic of high concentrations of NPs, takes effect. The agglomeration of the NPs reduces their effective surface area, thus reducing the hydrophilic sites in the membrane and the subsequent higher CA observed in PVDF 2.0 and PVDF 3.0 membranes. Agglomeration of the embedded nanoparticles also decreases the porosity of the membranes, which increases their CA, resulting in reduced hydrophilicity. A similar trend was observed by Vatanpour et al. [66] and Liang et al. [67]. Therefore, the Fe_3O_4-NPs loading of 1.0 wt% and below can be denoted as the viable amount to achieve improved hydrophilicity, and the PVDF 1.0 membrane exhibited the optimum hydrophilicity. In addition, the membranes' contact angle and their surface roughness are correlated according to the Wenzel model. The Wenzel model stipulated that the wettability of a surface is amplified by increasing its surface roughness [68]. Relating the surface roughness of the membranes with their CA, a trend of reduced CA is observed as the surface roughness increases. This confirms that their surface roughness might influence the membranes' hydrophilicity. Therefore, the hydrophilic nature of the Fe_3O_4-NPs and the membranes' surface roughness contribute to improving their hydrophilicity.

The hydrophilicity results correlate with the results of the porosity measurements shown in Table 3, which revealed that the porosity of the membranes increases with an increase in the Fe_3O_4-NPs loading of up to 1.0 wt%. The observed increase in porosity can also be attributed to the high hydrophilicity of the Fe_3O_4-NPs, which induces fast solvent and non-solvent exchange during the phase inversion, resulting in the formation of more pores in the membranes [69]. At Fe_3O_4-NPs loadings higher than 1 wt%, the opposite effect was seen due to the increase in the viscosity of the dope solutions at high NP concentration, leading to the reduction in the rate of the solvent and non-solvent exchange during the phase inversion, resulting to less porous membranes [70]. The decrease in porosity at high Fe_3O_4-NPs loadings was also facilitated by the blockage of the membrane's pores due to the agglomeration of the NPs at higher concentrations resulting in a less porous membrane.

The equilibrium water content (EWC) of the various membranes, also presented in Table 3, was consistent with their calculated porosity. An increase in EWC was obtained as the concentration of the Fe_3O_4-NPs in the membranes increased, indicating that the hydrophilicity of the Fe_3O_4-NPs plays a significant role in improving the EWC of membranes. The EWC of the pristine PVDF was 53.5 %, which increased to 75.5 % for the membrane modified with 1.0 wt% of Fe_3O_4-NPs. Above 1.0 wt% of Fe_3O_4-NPs loading, the EWC of the membrane decreases, which could also be explained by the agglomeration of the highly concentrated Fe_3O_4-NPs leading to the blockage of membrane pores and the eventual decrease in the EWC of the membranes.

The zeta potentials of the membranes at various pH are shown in Fig. 9(b), and it describes the nature of the charges of the membranes at the measured pH of the solution; hence, it plays a vital role in predicting the performance of membranes at varying pH [31]. The isoelectric point (IEP) of the pristine membrane was observed at pH 4.3. The Fe_3O_4-NPs/PVDF membranes have positive zeta potentials at low pH, which becomes negative at higher pH. This observed trend can be attributed to the tendency of metal oxide nanoparticles to hydrate in aqueous solution, and the surface functional groups of the hydrated metal oxide can be protonated or deprotonated depending on the pH of the solution [71].

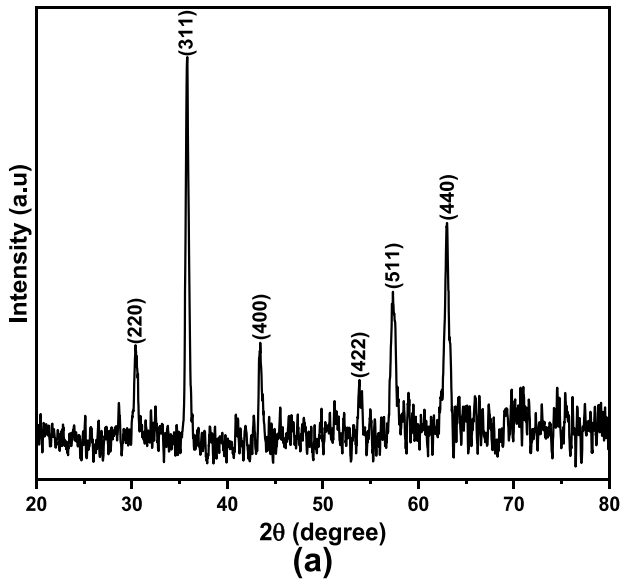

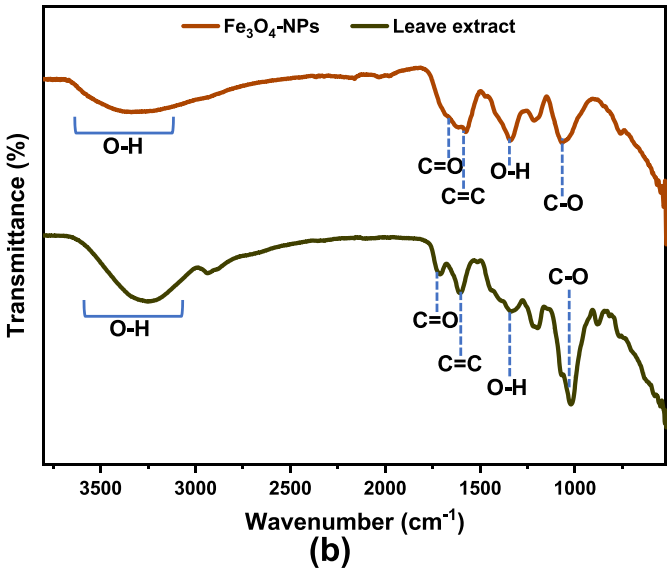

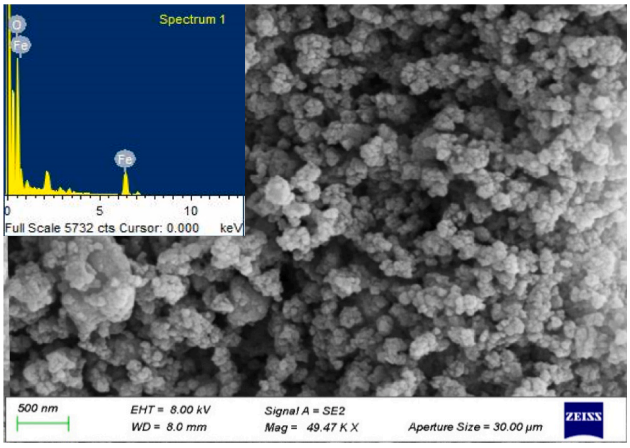

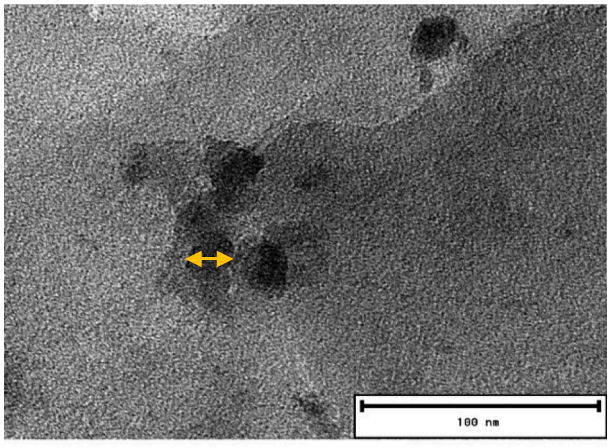

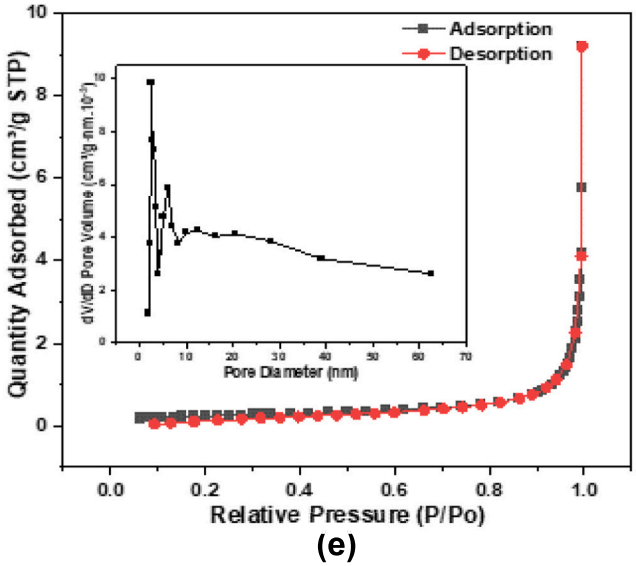

Fig. 2. (a) XRD pattern, (b) FTIR spectra, (c) SEM image, (d) TEM image, and (e) N_2 adsorption-desorption isotherm and pore size distribution (inset) of the Fe_3O_4-NPs.

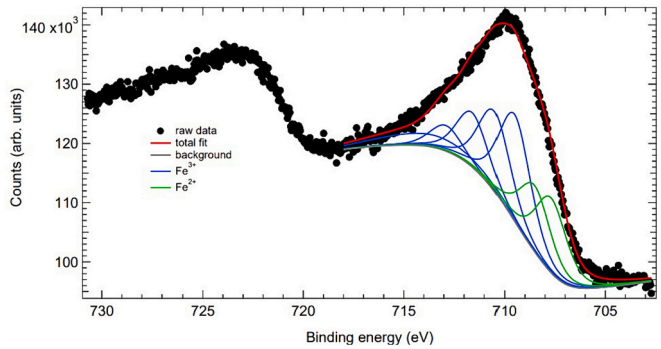

Fig. 3. XPS spectra of the Fe 2p core level.

Thus, the hydrated Fe_3O_4-NPs in the membrane were either protonated or deprotonated at low or high pH, resulting in the positive or negative charge observed for the modified membrane at the various pH ranges.

The mechanical property of the membranes is an essential factor that can determine their practical application in terms of their ability to withstand various operational conditions that the membranes will be subjected to during their usage in the treatment of wastewater [26]. Thus, the mechanical properties of the fabricated membranes with different loadings of the Fe_3O_4-NPs were investigated using a Tesla analyzer and are shown in the stress-strain curves in Fig. 10(a). Significant improvement in the tensile strength of the membranes was seen as the Fe_3O_4-NPs were incorporated into the membranes. The ultimate tensile strength of the pristine PVDF was 3.17 MPa, while the PVDF 0.2 and PVDF 1.0 had a tensile strength of 4.46 MPa and 4.24 MPa, respectively. The observed improvement in the tensile strength of the membranes is due to the inherent rigidity of the nanoparticles, which enhanced their stiffness. As the FTIR spectra of the NPs in Fig. 2 (b) show the presence of the -OH group in the NPs, there may be dipole-dipole bonding of the -OH group in the Fe_3O_4-NPs and the polar -CF group in the matrix of the modified membranes which could contribute to enhancing the mechanical stability of the membrane, hence the observed increase in tensile strength. A further increase in the Fe_3O_4-NPs loadings led to a decline in the tensile strength of the membrane, as seen in the lower tensile strength of PVDF 3.0, which could be due to agglomeration of the NPs at higher loading. The agglomeration reduces the interfacial area between the NPs and the PVDF matrix [72]. Thus, the effective fraction of the Fe_3O_4-NPs in the membrane matrix was reduced, resulting in the NPs' lesser ability to provide stiffness to the membranes.

A decrease in the strain at break was observed for all the membranes incorporated with the Fe_3O_4-NPs. This is expected as the Fe_3O_4-NPs introduce rigidity to the membranes, which minimizes their stretching capacity, resulting in the lower strain at break observed for the modified membranes.

The effect of the different Fe_3O_4-NPs loading on the thermal stability of the membranes, measured using TGA, is shown in Fig. 10(b). All the membranes exhibited a single-step degradation between 440 °C and 500 °C. The degradation temperature of the pristine membrane was 440 °C, which increased slightly to 456 °C as 0.2 wt% and 1 wt% of the Fe_3O_4-NPs were embedded into the PVDF membrane. This indicates a moderate improvement in the thermal stability of the membranes as the loading amount of the Fe_3O_4-NPs was increased. The significant weight loss between the region 440 °C and 500 °C is due to the decomposition of the PVDF polymers. At 800 °C, the mass of the residuals remaining after the decomposition of the PVDF is 6.94 %, 16.25 %, 21.95 %, and 22.7 % for PVDF 0, PVDF 0.2, PVDF 1.0, and PVDF 3.0, respectively. The incremental order of the residuals, which consist of carbon and the embedded Fe_3O_4-NPs, correlates with the increasing amount of the NPs across PVDF 0 to PVDF 3.0.

3.3. Membrane performance evaluation

3.3.1. Pure water and BTEX permeation performance

The effect of the Fe_3O_4-NPs loadings on the membrane flux was investigated by measuring the pure water flux (PWF) and BTEX flux of the membranes at different TMP. Fig. 11(a) depicts the PWF of the PVDF 0, PVDF 0.2, PVDF 1.0, and PVDF 3.0 membranes, and their respective BTEX flux is shown in Fig. 11(b). 100 ppm (of each component) of BTEX solution was used to evaluate the BTEX flux. The result shows that the

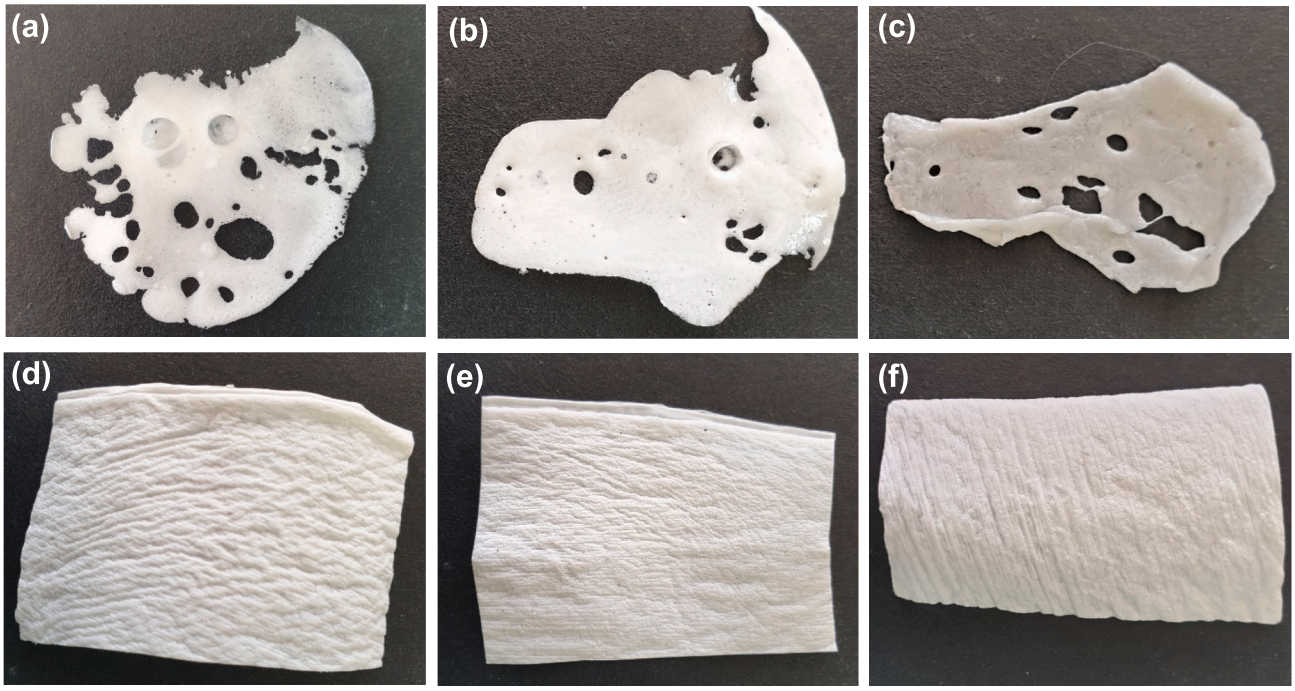

Fig. 4. The images of the PSF and PVDF membranes after exposure to BTEX solutions. PSF exposed to BTEX concentration of (a) 500 ppm, (b) 1000 ppm, and (c) 2000 ppm. PVDF exposed to BTEX concentration of (d) 500 ppm, (e) 1000 ppm, and (f) 2000 ppm.

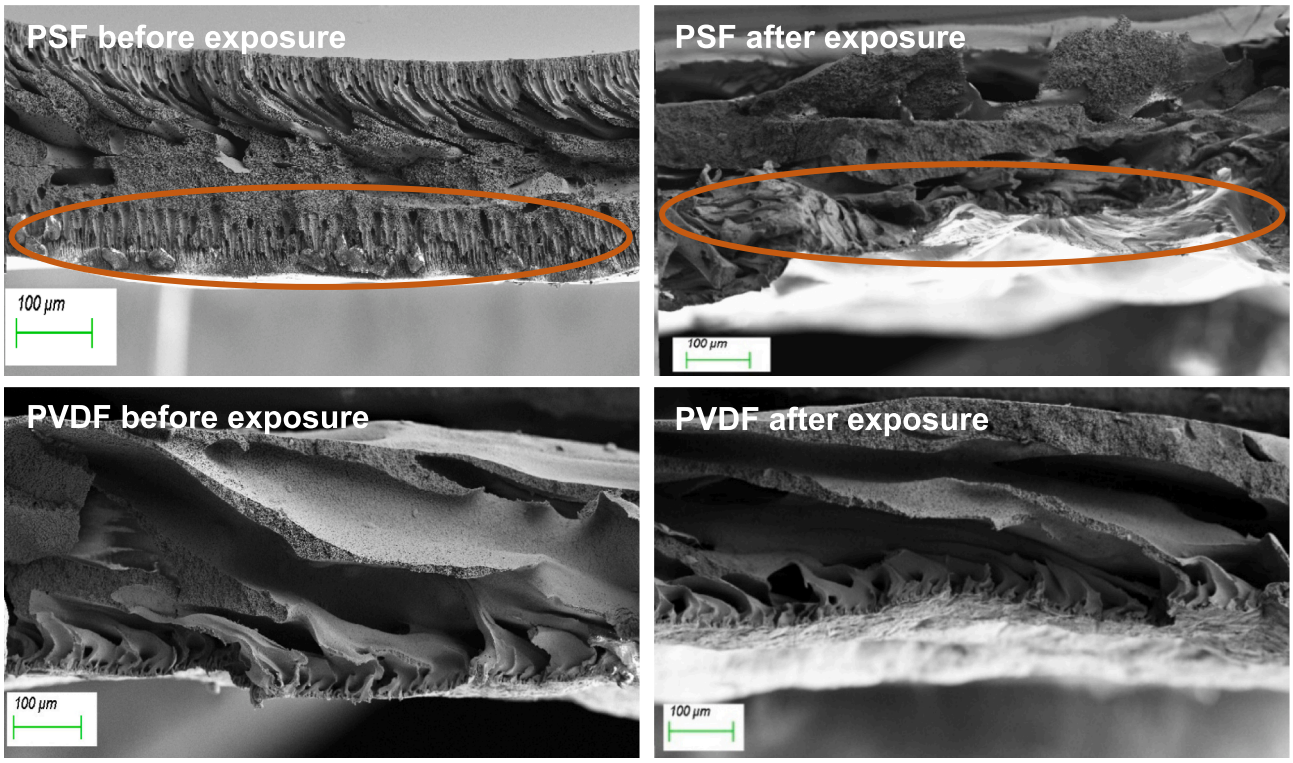

Fig. 5. SEM images of the before and after-exposure of PSF and PVDF membrane to BTEX solution.

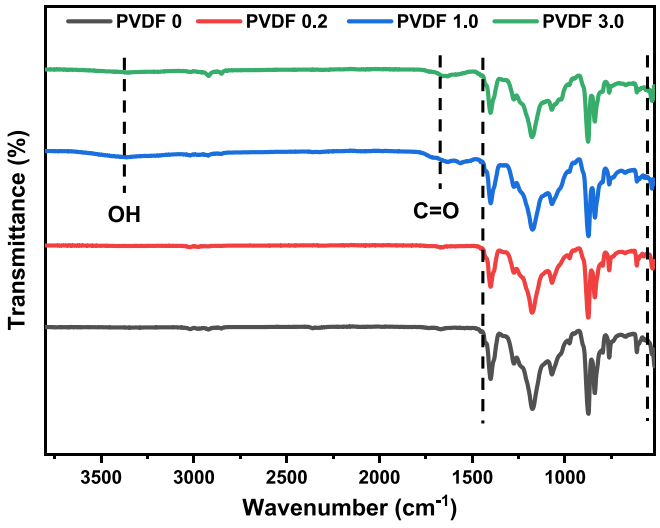

Fig. 6. FTIR spectra of the fabricated membranes.

PWF and the BTEX flux of all the membranes increased linearly as the TMP was increased, and all the Fe_3O_4-NPs/PVDF membranes exhibited higher PWF and BTEX flux than the pristine membrane. The observed improvement in the flux of the Fe_3O_4-NPs/PVDF membranes is due to the improved porosity of the membranes and the intrinsic hydrophilic nature of the Fe_3O_4-NPs, which reduced the water permeation resistance of the membranes. The porous nature of the Fe_3O_4-NPs, previously depicted in Fig. 2(e), also provided more hydrophilic nanochannels for improved water permeation through the membranes. While the increase in the PWF and BTEX flux of PVDF 0.2 and PVDF 1.0 is consistent with their Fe_3O_4-NPs loadings, the PWF and BTEX flux of PVDF 3.0 did not correlate with the amount of its Fe_3O_4-NPs loading because both fluxes of PVDF 3.0 were lower than that of the PVDF 0.2 and PVDF 1.0 across all the applied TMP. This dramatic decline in the fluxes of PVDF 3.0 could be attributed to the agglomeration of the Fe_3O_4-NPs as seen in its SEM image, which reduced the effective hydrophilic surface area of the embedded nanoparticles in the polymer matrix [73,74]. The agglomerated Fe_3O_4-NPs also blocked the membrane's pores, thereby intensifying the membrane's water permeation resistance. A similar trend was observed by Dadari et al. [75] in which a nickel-bentonite nanoparticles loading of 1.0 wt% led to the agglomeration of the nanoparticles in the membrane matrix, resulting in reduced PWF.

The BTEX flux of all the tested membranes was lower than their respective PWF across all the TMP, with the pristine membrane having the highest flux reduction. Among all the Fe_3O_4-NPs modified membranes, the PVDF 1.0 exhibited the lowest flux reduction across all the applied TMP. For instance, at a TMP of 300 kPa, the flux reduction of PVDF 1.0 was 35 %, while that of PVDF 0.2 and PVDF 3.0 were 38 % and 42 %, respectively. This could be explained by the better dispersion of the embedded nanoparticles in PVDF 1.0, which resulted in less pore tightening due to agglomerated nanoparticles. Hence, pore blockage of the PVDF 1.0 membrane by BTEX during the filtration is minimized, resulting in less permeation resistance. Hence, from the result of the evaluation of the PWF and BTEX flux of the membranes at the different Fe_3O_4-NPs loadings, the PVDF 1.0 membrane has the optimal flux among all the fabricated membranes; thus, 1.0 wt% of the NPs can be established as the optimum amount of the NPs that should be blended into a PVDF membrane to achieve an improvement in its flux.

3.3.2. *BTEX removal from synthetic BTEX water*

The effect of the Fe_3O_4-NPs loadings on the membranes' separation performance was ascertained by measuring the %R of BTEX by the different fabricated membranes. Since the separation performance of membranes is influenced by operational conditions such as TMP and concentrations [76,77], the BTEX rejection tests were performed at varying TMP and BTEX concentrations.

As presented in Fig. 12, all the Fe_3O_4-NPs/PVDF membranes exhibited higher BTEX rejection than the pristine membrane across all

the applied TMP, with an increase in the membranes' BTEX rejection capacity as the Fe_3O_4-NPs amount increases. This establishes the role of the Fe_3O_4-NPs in acting as both hydrophilic modifiers and nanofillers in the membrane matrix. With the surface of the membrane being hydrophilic, a hydration layer was formed on the membrane, which acted as an extra separation barrier. In addition, the BTEX rejection was in the order $B < T < E \leq X$, which suggests that the BTEX contaminants that might have penetrated through the hydration layer were removed through size exclusion. This is because the rejection pattern seems to correlate with the molecular diameters of B, T, E, and X, which are 0.58, 0.60, 0.63, and 0.63 nm, respectively [78]; hence, the NPs nanofillers might have contributed to the pore tightening of the membrane, as a consequence, the BTEX rejection was increased as the NPs loadings increase. Although the flux of PVDF 3.0, depicted in Fig. 11, was the lowest, the performance of PVDF 3.0 in terms of its BTEX rejection capacity improved, as seen in its higher BTEX rejection across all the TMP. Since agglomeration of NPs significantly reduces the membranes' free volume and creates extra barriers in their matrix [79], the higher BTEX rejection seen in PVDF 3.0 could be attributed to the agglomerated Fe_3O_4-NPs presented previously in the SEM image of the membrane. The agglomerated Fe_3O_4-NPs further tighten the membrane pores, resulting in the enhanced separation barrier of the PVDF 3.0 membrane.

Increasing the TMP led to a reduction in the BTEX rejection capacity of all the membranes as seen in Fig. 12. For instance, the %R of the PVDF 1.0 membrane for B are 73.2 %, 70.2 %, and 61.4 % at 100 kPa, 300 kPa, and 500 kPa respectively; for T are 75.5 %, 72.5 %, and 66.1 % at 100 kPa, 300 kPa, and 500 kPa respectively; for E are 80.0 %, 79.1 %, and 70.6 % at 100 kPa, 300 kPa, and 500 kPa respectively; for X are 80.5 %,

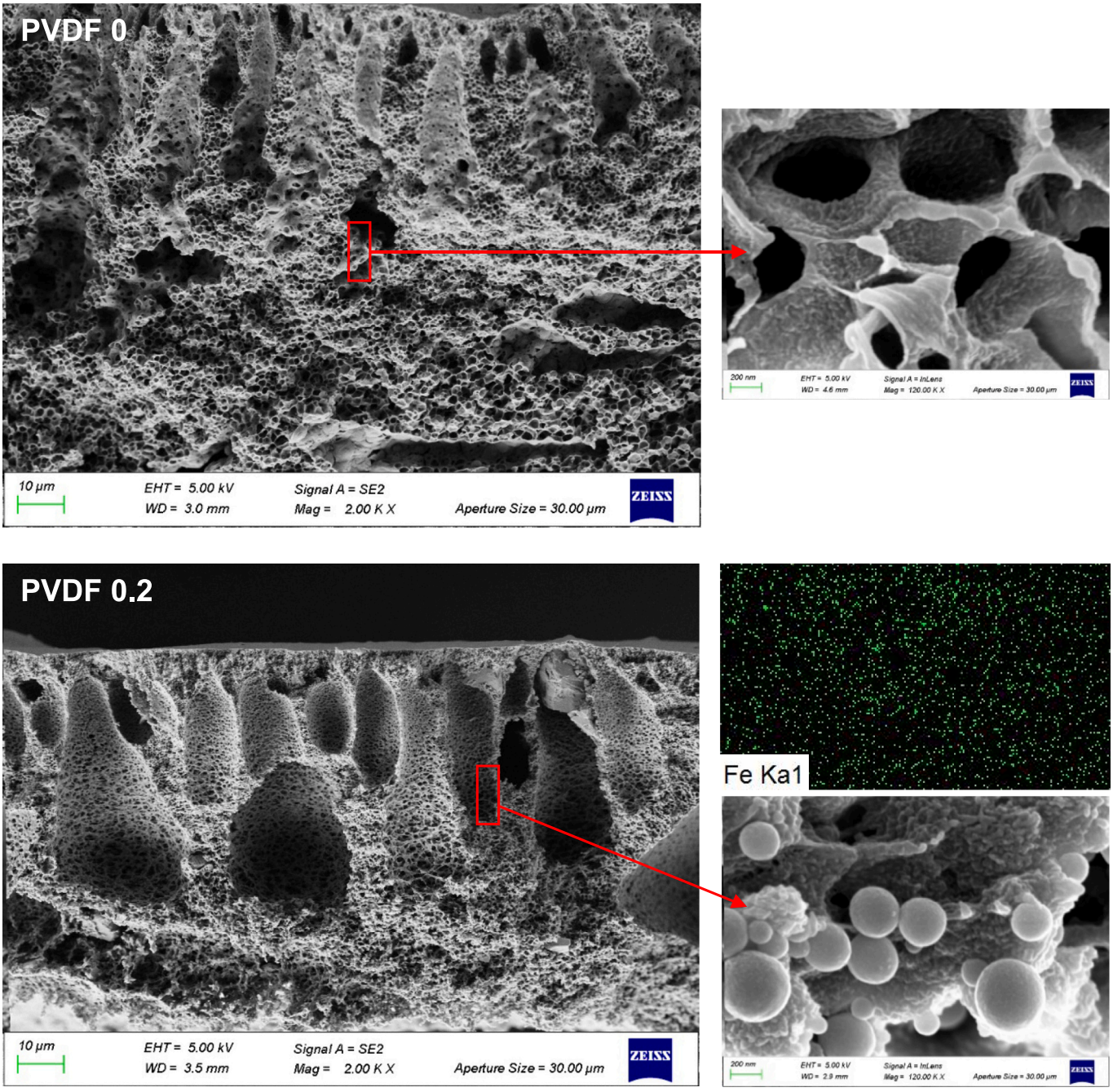

Fig. 7. Cross-section SEM images of fabricated membranes with their respective EDX mapping images.

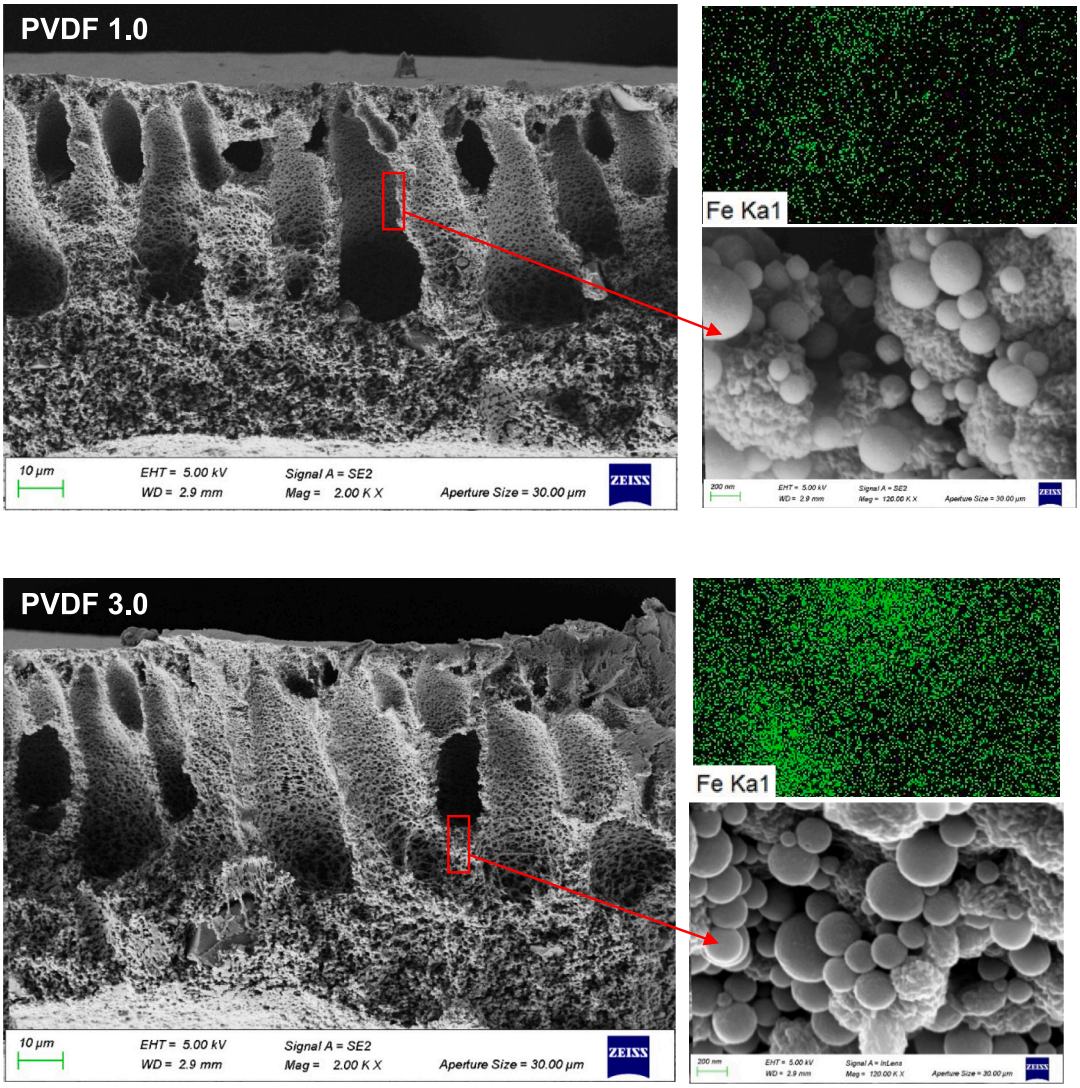

Fig. 7. (*continued*).

79.2 %, and 71.0 % at 100 kPa, 300 kPa, and 500 kPa respectively. Thus, under higher pressure, there was a higher chance of the contaminants penetrating through the hydration layer and the membrane due to the increased applied force, resulting in the observed decline in rejection as pressure increased. A similar observation was made by Wu et al. [80] when the rejection of bisphenol A and norfloxacin through an ultrafiltration membrane was tested under various TMPs.

To achieve good BTEX rejection using the membranes fabricated in this study, low TMP should be used during the filtration process. Considering both the membranes' BTEX flux and their BTEX rejection, 300 kPa can be designated as an ideal TMP where a reasonable tradeoff between flux and selectivity is achieved. Hence, 300 kPa is selected as the optimum TMP for the fabricated membranes.

The effect of the BTEX concentration on the rejection capacity of the membranes was studied at 300 kPa by filtering 200 mL of 50 ppm, 100 ppm, 150 ppm, and 200 ppm of BTEX solutions through the membranes under constant stirring. As shown in Fig. 13, the BTEX rejection capacity of all the Fe_3O_4-NPs/PVDF membranes increased as the BTEX concentration increased from 50 ppm to 100 ppm and remained relatively constant on further increase of the BTEX concentration. The constant rejection exhibited at higher BTEX concentrations can be explained by the accumulation of the BTEX on the membranes, which intensifies at the higher BTEX concentrations, thereby acting as an extra separation layer, resulting in the subsequent deposition of the BTEX on this layer. A similar trend was observed by Wu et al. [80] on the effect of feed concentration on the rejection of other organic contaminants, bisphenol A and norfloxacin, using ultrafiltration membranes.

Hence, the fabricated membranes can maintain stable BTEX separation without a decline in membrane rejection efficiency at the studied BTEX concentrations and feed volume.

3.3.3. *Antifouling and reusability study*

The effect of the various Fe_3O_4-NPs loadings on the antifouling ability of the tested membranes is shown in Fig. 14(a). The total fouling ratios of the modified membranes are lower than that of the pristine membrane, with the PVDF 1.0 having the lowest total fouling ratio of 36.3 %, which indicates about 30 % improvement in fouling reduction compared to the pristine membrane. The improvement in the antifouling tendency of the modified membranes could be attributed to the reduction in the hydrophobic nature of the membranes by introducing the hydrophilic Fe_3O_4-NPs into the membrane. Hydrophobic membranes are known to exacerbate fouling during the treatment of organic contaminated wastewater, while hydrophilic membranes reduce fouling by forming a hydration layer on the membranes, thereby minimizing the non-specific interaction of the foulants on the membranes [81].

The antifouling results also show that most of the fouling occurring during the BTEX filtration is irreversible, which could be a result of the penetration and trapping of the BTEX on the inner pores of the

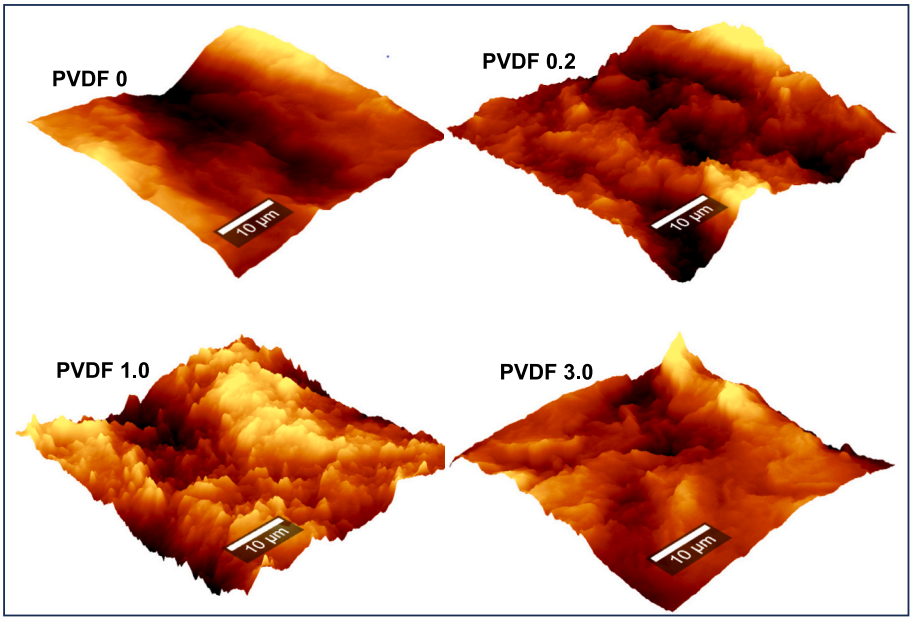

Fig. 8. Surface roughness images of the membranes.

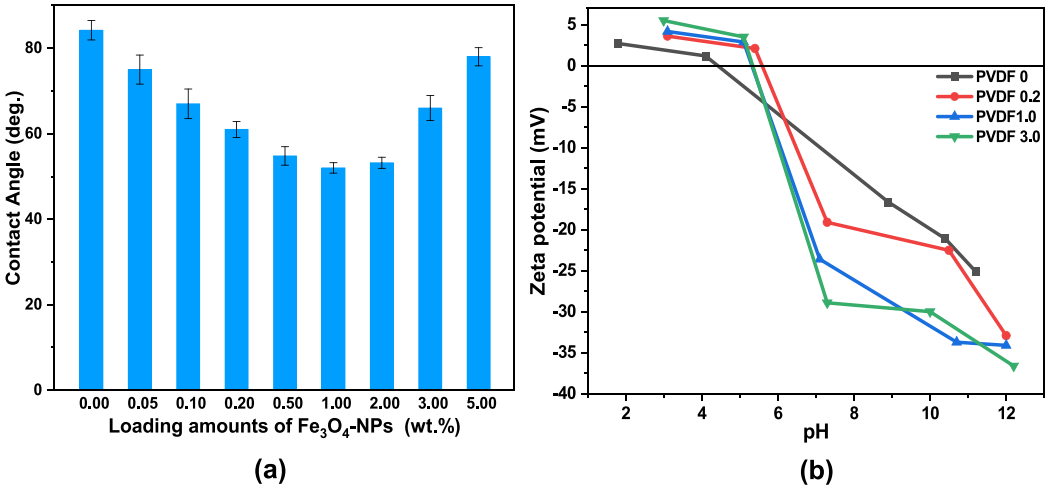

Fig. 9. (a) Contact angle values as a function of the Fe_3O_4-NPs loadings and (b) zeta potential of the tested membranes.

membranes, leading to less success in its removal through physical cleaning. The irreversibility of the fouling decreases as the Fe_3O_4 loading increases up to 1.0 wt%, which signifies that the incorporated nanoparticles significantly reduce the non-specific adsorption of BTEX on the membranes. PVDF 1.0 membrane was the only membrane whose reversible fouling was higher than its irreversible fouling. Hence, the membrane can be assigned an optimum performance based on its better ease of physical cleaning. The FRR of the PVDF 1.0 membrane was 81 %, which is the highest among all the membranes, which further shows its better performance in the recovery of its flux after fouling through physical cleaning.

The reusability of the membranes was evaluated by performing two cycles of BTEX filtration. Each cycle was followed by cleaning using backwashing with water, mild sonication in water, and then pure water filtration. Despite thoroughly cleaning the membranes, all the membranes exhibited a slight decline in PWF after each BTEX filtration and cleaning, as shown in Fig. 14(b). This could be due to the irreversible fouling that was established to be present in all the membranes during the antifouling test (Fig. 14a). The irreversible fouling is a result of stronger interactions between the BTEX and the membranes, which could not be easily removed by physical cleaning [60]. The penetration of the BTEX in the pores of the embedded Fe_3O_4-NPs in the modified membranes might also reduce the effectiveness of using physical cleaning to regenerate the modified membranes because of the small pore sizes of the Fe_3O_4-NPs which would make it difficult to remove the BTEX through physical cleaning. With the gradual decline of flux, the membranes may eventually lose their performance and require chemical cleaning to re-establish their performance.

3.3.4. Comparison with literature

Table 4 presents the comparison of this work with other studies that used modified membranes for the treatment of BTEX wastewater. It is important to note that this may not totally reflect the direct comparison of the performance of the various membranes due to the different filtration conditions used in the studies. However, the Fe_3O_4-NPs/PVDF membrane exhibited a better pure water flux than the other studies. The %R in Table 4 depicts the highest reported rejection of any of the components of BTEX, i.e., benzene, toluene, ethylbenzene, and xylene. The Fe_3O_4-NPs/PVDF membrane showed a high %R and FRR. Overall, the comparison of this study with other similar studies revealed the

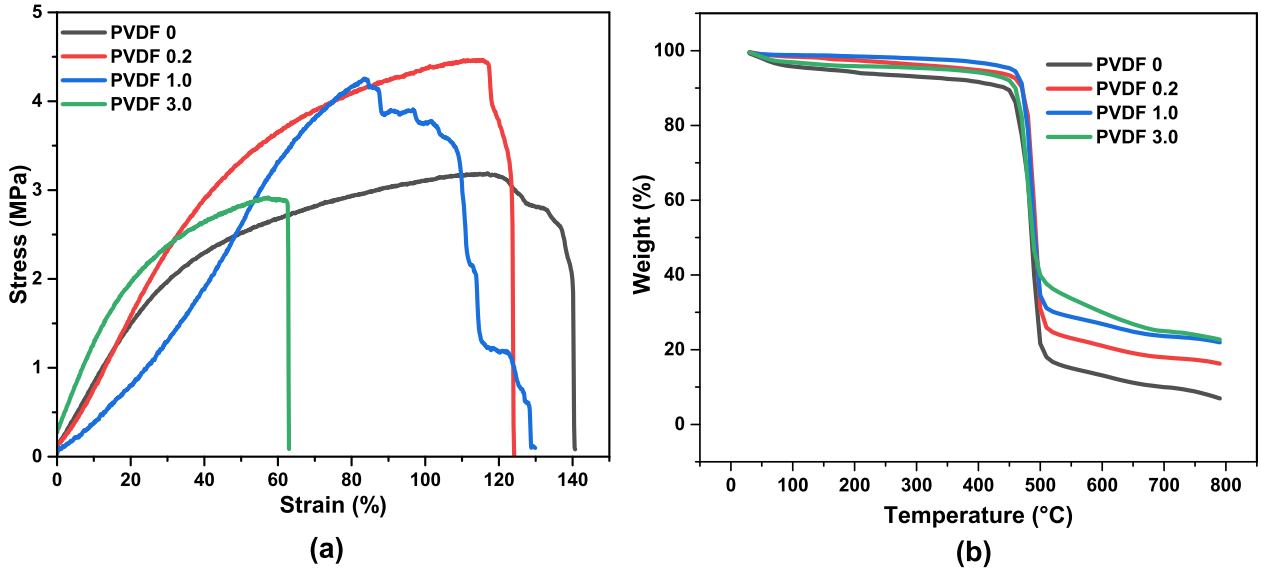

Fig. 10. (a) Stress-strain curves, and (b) TGA curves of the tested membranes.

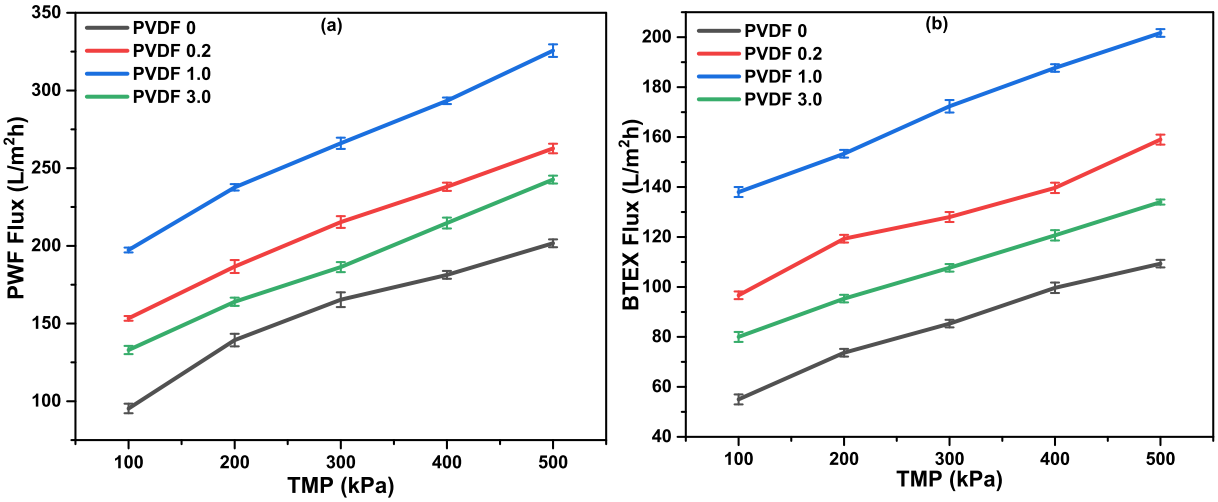

Fig. 11. (a) Pure water flux and (b) BTEX flux of the tested membranes.

Fe_3O_4-NPs/PVDF membrane as a potential membrane for removing BTEX from wastewater.

4. Conclusion

Hydrophilic and porous Fe_3O_4-NPs, synthesized using the aqueous extract of pomegranate leaves, were used to modify PVDF membranes to improve the membrane's performance towards BTEX removal. The SEM and AFM results show that the Fe_3O_4-NPs/PVDF membranes exhibited longer finger-like pores and rougher surfaces. The water contact angle decreased from 84.2° (pristine PVDF membrane) to 52.0° for the membrane modified with 1 wt% of the Fe_3O_4-NPs. Above 1 wt%, the water contact angle increased, thus suggesting that 1 wt% of the Fe_3O_4-NPs is optimal for improving the membrane hydrophilicity. The PWF and BTEX flux also improved, with the PVDF 1.0 exhibiting the optimum performance in this regard. The fluxes also increased as the TMP increased. PVDF 3.0 showed the highest BTEX rejection among all the fabricated membranes, and the rejection decreased as the TMP was increased. The Fe_3O_4-NPs/PVDF membranes also showed good anti-fouling propensity, with PVDF 1.0 having the highest FRR of 81 %. Overall, the Fe_3O_4-NPs/PVDF membranes presented improved filtration, separation, and antifouling performance, identifying them as potential membranes for BTEX removal from wastewater.

CRediT authorship contribution statement

Ngozi Enemuo: Data curation, Formal analysis, Investigation, Methodology, Visualization, Writing – original draft. **Heidi Richards:** Conceptualization, Funding acquisition, Methodology, Supervision, Writing – review & editing. **Michael O. Daramola:** Conceptualization, Formal analysis, Funding acquisition, Methodology, Project administration, Resources, Supervision, Validation, Writing – review & editing.

Declaration of competing interest

The authors declare that they have no known competing financial interests or personal relationships hat could have appeared to influence the work reported in this paper.

Data availability

Data will be made available on request.

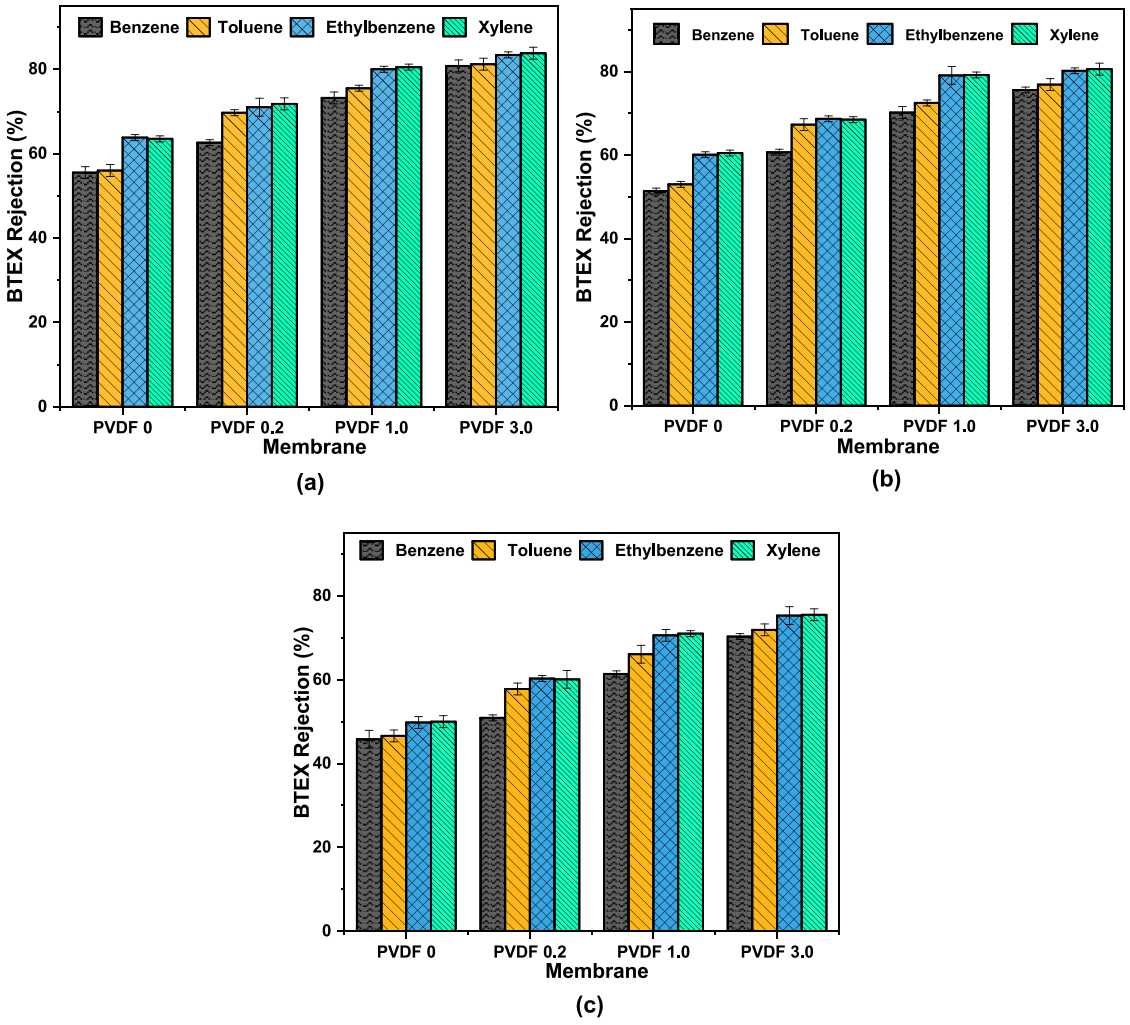

Fig. 12. Effect of TMP on the BTEX rejection of the membranes at (a) 100 kPa, (b) 300 kPa, and (c) 500 kPa.

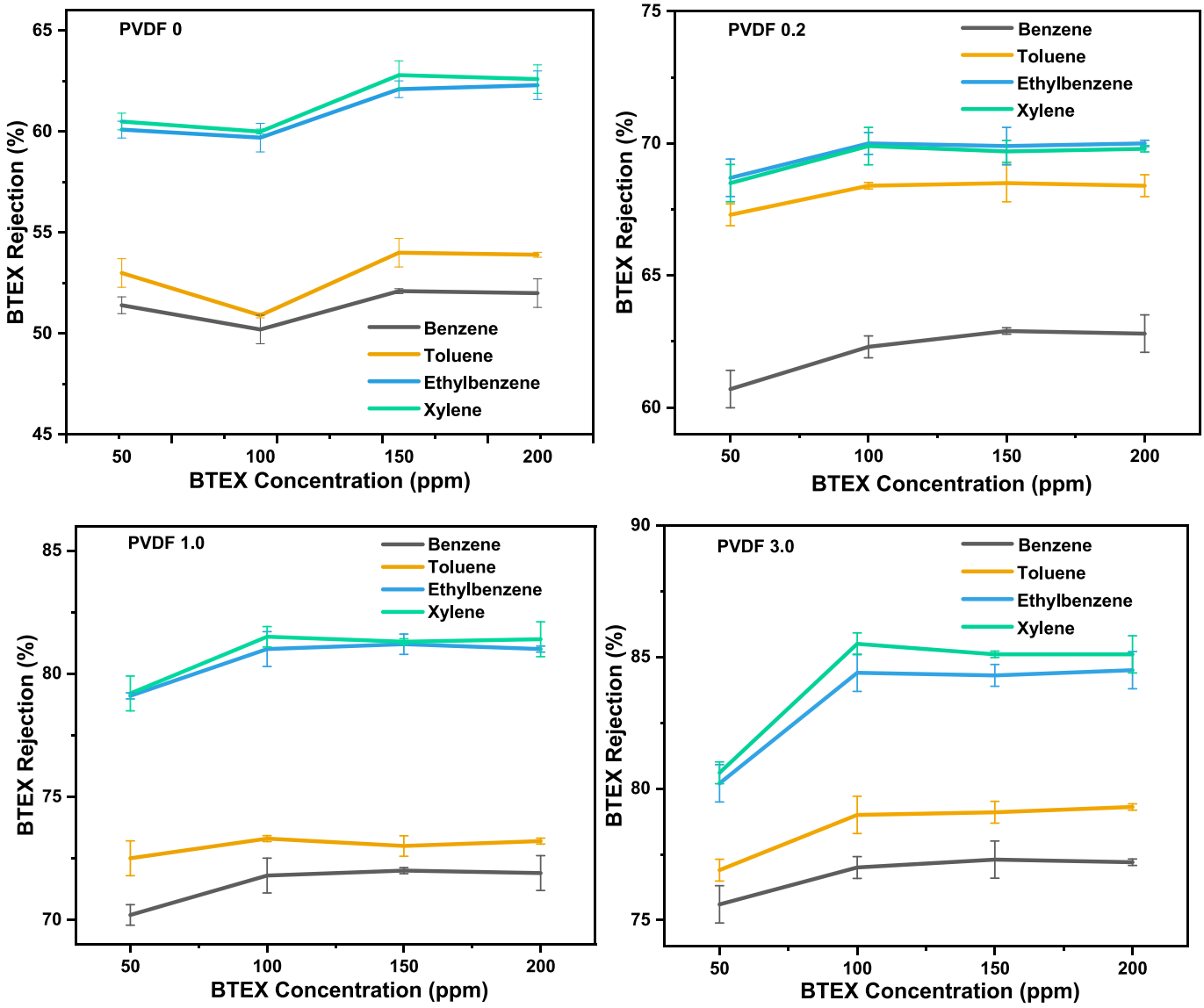

Fig. 13. Effect of BTEX concentrations on membranes' rejection capacity.

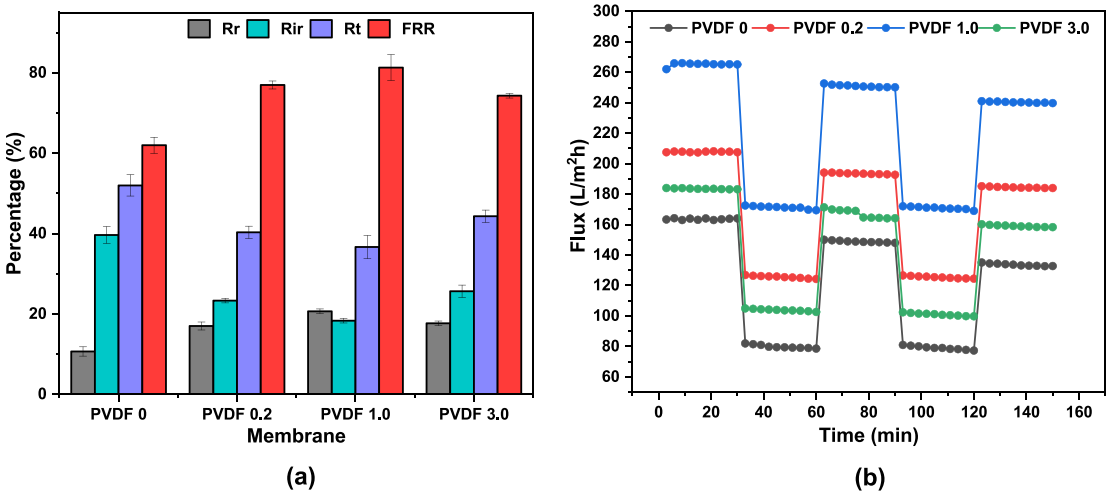

Fig. 14. (a) fouling resistance of the membranes, (b) Fluctuation of the flux of pure water and BTEX water over time.

Acknowledgments

The University of the Witwatersrand South Africa supported this research through the Postgraduate Merit Awards.

References

[1] H. Freeman, T. Harten, J. Springer, P. Randall, M.A. Curran, K. Stone, Industrial pollution prevention! A critical review, J. Air Waste Manage. Assoc. 42 (5) (1992) 618–656, https://doi.org/10.1080/10473289.1992.10467016.
[2] F.N. Chaudhry, M.F. Malik, Factors Affecting Water Pollution: a Review, J. Ecosyst. Ecography 7 (2017) 1, https://doi.org/10.4172/2157-7625.1000225.
[3] P. Wang, J. Yao, G. Wang, F. Hao, S. Shrestha, B. Xue, G. Xie, Y. Peng, Exploring the application of artificial intelligence technology for identification of water pollution characteristics and tracing the source of water quality pollutants, Sci. Total Environ. 693 (2019) 133440, https://doi.org/10.1016/j.scitotenv.2019.07.246.
[4] A. Butkovskyi, H. Bruning, S.A.E. Kools, H.H.M. Rijnaarts, A.P. Van Wezel, Organic pollutants in shale gas flowback and produced waters: identification, potential ecological impact, and implications for treatment strategies, Environ. Sci. Technol. 51 (9) (2017) 4740–4754, https://doi.org/10.1021/acs.est.6b05640.
[5] R. Yusta-García, M. Orta-Martínez, P. Mayor, C. González-Crespo, A. Rosell-Melé, Water contamination from oil extraction activities in Northern Peruvian Amazonian rivers, Environ. Pollut. 225 (2017) 370–380, https://doi.org/10.1016/j.envpol.2017.02.063.
[6] C.J. Davidson, J.H. Hannigan, S.E. Bowen, Effects of inhaled combined Benzene, Toluene, Ethylbenzene, and Xylenes (BTEX): toward an environmental exposure model, Environ. Toxicol. Pharmacol. 81 (2021) 103518, https://doi.org/10.1016/j.etap.2020.103518.
[7] S.-T. Lee, C.T. Vu, C. Lin, K.-S. Chen, High occurrence of BTEX around major industrial plants in Kaohsiung, Taiwan, Environ. Forensic 19 (3) (2018) 206–216, https://doi.org/10.1080/15275922.2018.1475432.
[8] B. Yu, Z. Yuan, Z. Yu, F. Xue-song, BTEX in the environment: An update on sources, fate, distribution, pretreatment, analysis, and removal techniques, Chem. Eng. J. 435 (2022) 134825, https://doi.org/10.1016/j.cej.2022.134825.
[9] USEPA, U.S. Environmental Protection Agency | US EPA. https://www.epa.gov/, 2023.
[10] A.L. Bolden, C.F. Kwiatkowski, T. Colborn, New look at BTEX: are ambient levels a problem? Environ. Sci. Technol. 49 (9) (2015) 5261–5276, https://doi.org/10.1021/es505316f.
[11] T. Lueders, The ecology of anaerobic degraders of BTEX hydrocarbons in aquifers, FEMS Microbiol. Ecol. 93 (1) (2017) fiw220, https://doi.org/10.1093/femsec/fiw220.
[12] P. Ekins, R. Vanner, J. Firebrace, Zero emissions of oil in water from offshore oil and gas installations: economic and environmental implications, J. Clean. Prod. 15 (13) (2007) 1302–1315, https://doi.org/10.1016/j.jclepro.2006.07.014.
[13] Y. Mikhak, M.M.A. Torabi, A. Fouladitajar, Chapter 3—refinery and petrochemical wastewater treatment, in: C.M. Galanakis, E. Agrafioti (Eds.), Sustainable Water and Wastewater Processing, Elsevier, 2019, pp. 55–91, https://doi.org/10.1016/B978-0-12-816170-8.00003-X.
[14] S. Zha, G. Zhang, N. Dawson, J. Yu, N. Liu, R. Lee, Study of PVDF/Si-R hybrid hollow fiber membranes for removal of dissolved organics from produced water by membrane adsorption, Sep. Purif. Technol. 163 (2016) 290–299, https://doi.org/10.1016/j.seppur.2016.03.003.
[15] K.T. Amakiri, A.R. Canon, M. Molinari, A. Angelis-Dimakis, Review of oilfield produced water treatment technologies, Chemosphere 298 (2022) 134064, https://doi.org/10.1016/j.chemosphere.2022.134064.
[16] E.T. Igunnu, G.Z. Chen, Produced water treatment technologies, Int. J. Low-Carbon Technol. 9 (3) (2014) 157–177, https://doi.org/10.1093/ijlct/cts049.
[17] N.K. Khanzada, M.U. Farid, J.A. Kharraz, J. Choi, C.Y. Tang, L.D. Nghiem, A. Jang, A.K. An, Removal of organic micropollutants using advanced membrane-based water and wastewater treatment: a review, J. Membr. Sci. 598 (2020) 117672, https://doi.org/10.1016/j.memsci.2019.117672.
[18] Y. Subasi, B. Cicek, Recent advances in hydrophilic modification of PVDF ultrafiltration membranes – a review: part II, Membr. Technol. 2017 (11) (2017) 5–11, https://doi.org/10.1016/S0958-2118(17)30233-1.
[19] D.J. Miller, D.R. Paul, B.D. Freeman, A crossflow filtration system for constant permeate flux membrane fouling characterization, Rev. Sci. Instrum. 84 (3) (2013) 035003, https://doi.org/10.1063/1.4794909.
[20] E. Tummons, Q. Han, H.J. Tanudjaja, C.A. Hejase, J.W. Chew, V.V. Tarabara, Membrane fouling by emulsified oil: a review, Sep. Purif. Technol. 248 (2020) 116919, https://doi.org/10.1016/j.seppur.2020.116919.
[21] B. Van der Bruggen, Chemical modification of polyethersulfone nanofiltration membranes: a review, J. Appl. Polym. Sci. 114 (1) (2009) 630–642, https://doi.org/10.1002/app.30578.
[22] G. Kang, Y. Cao, Application and modification of poly(vinylidene fluoride) (PVDF) membranes – a review, J. Membr. Sci. 463 (2014) 145–165, https://doi.org/10.1016/j.memsci.2014.03.055.
[23] D.J. Miller, D.R. Dreyer, C.W. Bielawski, D.R. Paul, B.D. Freeman, Surface modification of water purification membranes, Angew. Chem. Int. Ed. 56 (17) (2017) 4662–4711, https://doi.org/10.1002/anie.201601509.
[24] J. Yin, B. Deng, Polymer-matrix nanocomposite membranes for water treatment, J. Membr. Sci. 479 (2015) 256–275, https://doi.org/10.1016/j.memsci.2014.11.019.
[25] S. Al Aani, C.J. Wright, M.A. Atieh, N. Hilal, Engineering nanocomposite membranes: addressing current challenges and future opportunities, Desalination 401 (2017) 1–15, https://doi.org/10.1016/j.desal.2016.08.001.
[26] S. Al Aani, C.J. Wright, M.A. Atieh, N. Hilal, Engineering nanocomposite membranes: addressing current challenges and future opportunities, Desalination 401 (2017) 1–15, https://doi.org/10.1016/j.desal.2016.08.001.
[27] C. Wang, M.J. Park, H. Yu, H. Matsuyama, E. Drioli, H.K. Shon, Recent advances of nanocomposite membranes using layer-by-layer assembly, J. Membr. Sci. 661 (2022) 120926, https://doi.org/10.1016/j.memsci.2022.120926.
[28] V. Vatanpour, M. Hazrati, M. Sheydaei, A. Dehqan, Investigation of using UV/H2O2 pre-treatment process on filterability and fouling reduction of PVDF/TiO2 nanocomposite ultrafiltration membrane, Chem. Eng. Process. Process Intensif. 170 (2022) 108677, https://doi.org/10.1016/j.cep.2021.108677.
[29] D. Zou, X. Chen, E. Drioli, X. Ke, M. Qiu, Y. Fan, Facile co-sintering process to fabricate sustainable antifouling silver nanoparticles (AgNPs)-enhanced tight ceramic ultrafiltration membranes for protein separation, J. Membr. Sci. 593 (2020) 117402, https://doi.org/10.1016/j.memsci.2019.117402.
[30] Y. Lin, C.H. Loh, L. Shi, Y. Fan, R. Wang, Preparation of high-performance Al2O3/PES composite hollow fiber UF membranes via facile in-situ vapor induced hydrolyzation, J. Membr. Sci. 539 (2017) 65–75, https://doi.org/10.1016/j.memsci.2017.05.069.
[31] J. Zhu, S. Zhou, M. Li, A. Xue, Y. Zhao, W. Peng, W. Xing, PVDF mixed matrix ultrafiltration membrane incorporated with deformed rebar-like Fe3O4–palygorskite nanocomposites to enhance strength and antifouling properties, J. Membr. Sci. 612 (2020) 118467, https://doi.org/10.1016/j.memsci.2020.118467.
[32] C.N. Matindi, M. Hu, S. Kadanyo, Q.V. Ly, N.N. Gumbi, D.S. Dlamini, J. Li, Y. Hu, Z. Cui, J. Li, Tailoring the morphology of polyethersulfone/sulfonated polysulfone ultrafiltration membranes for highly efficient separation of oil-in-water emulsions using TiO2 nanoparticles, J. Membr. Sci. 620 (2021) 118868, https://doi.org/10.1016/j.memsci.2020.118868.
[33] N. Kong, C. Chen, Q. Zeng, B. Li, L. Shen, H. Lin, Enriching Fe3O4@MoS2 composites in surface layer to fabricate polyethersulfone (PES) composite membrane: the improved performance and mechanisms, Sep. Purif. Technol. 302 (2022) 122178, https://doi.org/10.1016/j.seppur.2022.122178.
[34] Z.-H. Huang, X. Zhang, Y.-X. Wang, J.-Y. Sun, H. Zhang, W.-L. Liu, M.-P. Li, X.-H. Ma, Z.-L. Xu, Fe3O4/PVDF catalytic membrane treatment organic wastewater with simultaneously improved permeability, catalytic property and anti-fouling, Environ. Res. 187 (2020) 109617, https://doi.org/10.1016/j.envres.2020.109617.
[35] C.F. Unuigbe, O.M. Fayemiwo, M.O. Daramola, Performance evaluation of iron nanoparticles infused polyethersulphone (Fe-NPs/PES) membrane during treatment of BTEX-contaminated wastewater, Water Environ. J. 34 (S1) (2020) 74–86, https://doi.org/10.1111/wej.12506.
[36] T. Makhani, O.O. Sadare, S. Wagenaar, K. Moothi, R.M. Moutloali, M.O. Daramola, Fabrication and performance evaluation of tannin iron complex (TA-FeIII/PES) UF membrane in treatment of BTEX wastewater, Water SA 48 (4) (2022) Article 4.
[37] C.P.M. de Oliveira, I. Fernandes Farah, K. Koch, J.E. Drewes, M.M. Viana, M.C. S. Amaral, TiO2-Graphene oxide nanocomposite membranes: a review, Sep. Purif. Technol. 280 (2022) 119836, https://doi.org/10.1016/j.seppur.2021.119836.
[38] C. Ursino, R. Castro-Muñoz, E. Drioli, L. Gzara, M.H. Albeirutty, A. Figoli, Progress of nanocomposite membranes for water treatment, Membranes 8(2), Article 2 (2018), https://doi.org/10.3390/membranes8020018.
[39] X. Wei, Y. Liu, J. Zheng, X. Wang, S. Xia, B. Van der Bruggen, A critical review on thin-film nanocomposite membranes enabled by nanomaterials incorporated in different positions and with diverse dimensions: performance comparison and mechanisms, J. Membr. Sci. 661 (2022) 120952, https://doi.org/10.1016/j.memsci.2022.120952.
[40] X. Wei, Y. Liu, J. Zheng, X. Wang, S. Xia, B. Van der Bruggen, A critical review on thin-film nanocomposite membranes enabled by nanomaterials incorporated in different positions and with diverse dimensions: performance comparison and mechanisms, J. Membr. Sci. 661 (2022) 120952, https://doi.org/10.1016/j.memsci.2022.120952.
[41] G. Wypych, Handbook of Polymers, Elsevier, 2022.
[42] Q. Xu, W. Li, L. Ma, D. Cao, G. Owens, Z. Chen, Simultaneous removal of ammonia and phosphate using green synthesized iron oxide nanoparticles dispersed onto zeolite, Sci. Total Environ. 703 (2020) 135002, https://doi.org/10.1016/j.scitotenv.2019.135002.
[43] S. Ying, Z. Guan, P.C. Ofoegbu, P. Clubb, C. Rico, F. He, J. Hong, Green synthesis of nanoparticles: current developments and limitations, Environ. Technol. Innov. 26 (2022) 102336, https://doi.org/10.1016/j.eti.2022.102336.
[44] X. Chen, G. Huang, C. An, R. Feng, Y. Wu, C. Huang, Plasma-induced PAA-ZnO coated PVDF membrane for oily wastewater treatment: preparation, optimization, and characterization through Taguchi OA design and synchrotron-based X-ray analysis, J. Membr. Sci. 582 (2019) 70–82, https://doi.org/10.1016/j.memsci.2019.03.091.
[45] M. Nikbakht Fini, H.T. Madsen, J. Muff, The effect of water matrix, feed concentration and recovery on the rejection of pesticides using NF/RO membranes in water treatment, Sep. Purif. Technol. 215 (2019) 521–527, https://doi.org/10.1016/j.seppur.2019.01.047.
[46] M. Bandeira, M. Giovanela, M. Roesch-Ely, D.M. Devine, J. da Silva Crespo, Green synthesis of zinc oxide nanoparticles: a review of the synthesis methodology and mechanism of formation, Sustain. Chem. Pharm. 15 (2020) 100223, https://doi.org/10.1016/j.scp.2020.100223.
[47] A. Radoń, A. Drygała, Ł. Hawełek, D. Łukowiec, Structure and optical properties of Fe3O4 nanoparticles synthesized by co-precipitation method with different organic

modifiers, Mater. Charact. 131 (2017) 148–156, https://doi.org/10.1016/j.matchar.2017.06.034.
[48] V. Kumar, S. Singh, B. Srivastava, R. Bhadouria, R. Singh, Green synthesis of silver nanoparticles using leaf extract of Holoptelea integrifolia and preliminary investigation of its antioxidant, anti-inflammatory, antidiabetic and antibacterial activities, J. Environ. Chem. Eng. 7 (3) (2019) 103094, https://doi.org/10.1016/j.jece.2019.103094.
[49] N. Swilam, K.A. Nematallah, Polyphenols profile of pomegranate leaves and their role in green synthesis of silver nanoparticles, Sci. Rep. 10 (1) (2020) 1, https://doi.org/10.1038/s41598-020-71847-5.
[50] R.G. Saratale, H.S. Shin, G. Kumar, G. Benelli, D.-S. Kim, G.D. Saratale, Exploiting antidiabetic activity of silver nanoparticles synthesized using Punica granatum leaves and anticancer potential against human liver cancer cells (HepG2), Artif. Cells Nanomed. Biotechnol. 46 (1) (2018) 211–222, https://doi.org/10.1080/21691401.2017.1337031.
[51] N.P. Wickramaratne, V.S. Perera, B.-W. Park, M. Gao, G.W. McGimpsey, S. D. Huang, M. Jaroniec, Graphitic mesoporous carbons with embedded Prussian blue-derived Iron oxide nanoparticles synthesized by soft templating and low-temperature graphitization, Chem. Mater. 25 (14) (2013) 2803–2811, https://doi.org/10.1021/cm401124d.
[52] M.C. Biesinger, B.P. Payne, A.P. Grosvenor, L.W.M. Lau, A.R. Gerson, R.St. Smart, C., Resolving surface chemical states in XPS analysis of first row transition metals, oxides and hydroxides: Cr, Mn, Fe, Co and Ni, Appl. Surf. Sci. 257 (7) (2011) 2717–2730, https://doi.org/10.1016/j.apsusc.2010.10.051.
[53] A.P. Grosvenor, B.A. Kobe, M.C. Biesinger, N.S. McIntyre, Investigation of multiplet splitting of Fe 2p XPS spectra and bonding in iron compounds, Surf. Interface Anal. 36 (12) (2004) 1564–1574, https://doi.org/10.1002/sia.1984.
[54] N.S. McIntyre, D.G. Zetaruk, X-ray photoelectron spectroscopic studies of iron oxides, Anal. Chem. 49 (11) (1977) 1521–1529, https://doi.org/10.1021/ac50019a016.
[55] C. Ma, J. Hu, W. Sun, Z. Ma, W. Yang, L. Wang, Z. Ran, B. Zhao, Z. Zhang, H. Zhang, Graphene oxide-polyethylene glycol incorporated PVDF nanocomposite ultrafiltration membrane with enhanced hydrophilicity, permeability, and antifouling performance, Chemosphere 253 (2020) 126649, https://doi.org/10.1016/j.chemosphere.2020.126649.
[56] A. Alkhouzaam, H. Qiblawey, Novel polysulfone ultrafiltration membranes incorporating polydopamine functionalized graphene oxide with enhanced flux and fouling resistance, J. Membr. Sci. 620 (2021) 118900, https://doi.org/10.1016/j.memsci.2020.118900.
[57] A. Khan, T.A. Sherazi, Y. Khan, S. Li, S.A.R. Naqvi, Z. Cui, Fabrication and characterization of polysulfone/modified nanocarbon black composite antifouling ultrafiltration membranes, J. Membr. Sci. 554 (2018) 71–82, https://doi.org/10.1016/j.memsci.2018.02.063.
[58] Y. Du, B.K. Pramanik, Y. Zhang, V. Jegatheesan, Influence of molecular weight cut-off (MWCO) of commercial ultrafiltration substrate on the performance of thin film composite nanofiltration membrane, Desalination 541 (2022) 116020, https://doi.org/10.1016/j.desal.2022.116020.
[59] Y. Wang, H. Shen, C. Cui, L. Hou, W. Chen, Q. Liu, J. Xu, Z. Wang, J. Hu, Towards to better permeability and antifouling sulfonated poly (aryl ether ketone sulfone) with carboxyl group ultrafiltration membrane blending with amine functionalization of SBA-15, Sep. Purif. Technol. 265 (2021) 118512, https://doi.org/10.1016/j.seppur.2021.118512.
[60] T.A. Sherazi, S. Azam, S.H. Shah, S. Hussain, S.A.R. Naqvi, S. Li, Zwitterionic analog structured ultrafiltration membranes for high permeate flux and improved anti-fouling performance, J. Membr. Sci. 643 (2022) 120060, https://doi.org/10.1016/j.memsci.2021.120060.
[61] M.I. Baig, P.G. Ingole, J. Jeon, S.U. Hong, W.K. Choi, H.K. Lee, Water vapor transport properties of interfacially polymerized thin film nanocomposite membranes modified with graphene oxide and GO-TiO2 nanofillers, Chem. Eng. J. 373 (2019) 1190–1202, https://doi.org/10.1016/j.cej.2019.05.122.
[62] Y.H. Tan, P.S. Goh, A.F. Ismail, B.C. Ng, G.S. Lai, Decolourization of aerobically treated palm oil mill effluent (AT-POME) using polyvinylidene fluoride (PVDF) ultrafiltration membrane incorporated with coupled zinc-iron oxide nanoparticles, Chem. Eng. J. 308 (2017) 359–369, https://doi.org/10.1016/j.cej.2016.09.092.
[63] J. Rowley, N.H. Abu-Zahra, Synthesis and characterization of polyethersulfone membranes impregnated with (3-aminopropyltriethoxysilane) APTES-Fe3O4 nanoparticles for As(V) removal from water, J. Environ. Chem. Eng. 7 (1) (2019) 102875, https://doi.org/10.1016/j.jece.2018.102875.
[64] S. Akram, V. Naddeo, Z. Rehan, M. Zahid, A. Rashid, W. Razzaq, A comprehensive review on polymeric nano-composite membranes for water treatment, J. Membr. Sci. Technol. 08 (2018), https://doi.org/10.4172/2155-9589.1000179.
[65] Y. Liu, X. Wang, X. Gao, J. Zheng, J. Wang, A. Volodin, Y.F. Xie, X. Huang, B. Van der Bruggen, J. Zhu, High-performance thin film nanocomposite membranes enabled by nanomaterials with different dimensions for nanofiltration, J. Membr. Sci. 596 (2020) 117717, https://doi.org/10.1016/j.memsci.2019.117717.
[66] V. Vatanpour, M. Esmaeili, S. Chahvari, M. Masteri-Farahani, Evaluation of morphology, performance and fouling tendency of mixed matrix PVDF ultrafiltration membranes incorporated by different size-controlled SAPO-34 nanozeolites, J. Environ. Chem. Eng. 9 (5) (2021) 105900, https://doi.org/10.1016/j.jece.2021.105900.
[67] Z. Liang, J. Wang, Q. Zhang, T. Zhuang, C. Zhao, Y. Fu, Y. Zhang, F. Yang, Composite PVDF ultrafiltration membrane tailored by sandwich-like GO@UiO-66 nanoparticles for breaking the trade-off between permeability and selectivity, Sep. Purif. Technol. 276 (2021) 119308, https://doi.org/10.1016/j.seppur.2021.119308.
[68] R.N. Wenzel, Resistance of solid surfaces to wetting by water, Ind. Eng. Chem. 28 (8) (1936) 988–994, https://doi.org/10.1021/ie50320a024.
[69] J. Lin, W. Ye, K. Zhong, J. Shen, N. Jullok, A. Sotto, B. Van der Bruggen, Enhancement of polyethersulfone (PES) membrane doped by monodisperse Stöber silica for water treatment, Chem. Eng. Process. Process Intensif. 107 (2016) 194–205, https://doi.org/10.1016/j.cep.2015.03.011.
[70] E. Yuliwati, A.F. Ismail, Effect of additives concentration on the surface properties and performance of PVDF ultrafiltration membranes for refinery produced wastewater treatment, Desalination 273 (1) (2011) 226–234, https://doi.org/10.1016/j.desal.2010.11.023.
[71] N. Wang, C. Hsu, L. Zhu, S. Tseng, J.-P. Hsu, Influence of metal oxide nanoparticles concentration on their zeta potential, J. Colloid Interface Sci. 407 (2013) 22–28, https://doi.org/10.1016/j.jcis.2013.05.058.
[72] Y. Wu, F. Wang, Y. Huang, Facile and simple fabrication of strong, transparent and flexible aramid nanofibers/bacterial cellulose nanocomposite membranes, Compos. Sci. Technol. 159 (2018) 70–76, https://doi.org/10.1016/j.compscitech.2018.02.036.
[73] S.M. Hosseini, S. Sohrabnejad, G. Nabiyouni, E. Jashni, B. Van der Bruggen, A. Ahmadi, Magnetic cation exchange membrane incorporated with cobalt ferrite nanoparticles for chromium ions removal via electrodialysis, J. Membr. Sci. 583 (2019) 292–300, https://doi.org/10.1016/j.memsci.2019.04.069.
[74] T.-Y. Liu, Z.-H. Liu, R.-X. Zhang, Y. Wang, B.V. der Bruggen, X.-L. Wang, Fabrication of a thin film nanocomposite hollow fiber nanofiltration membrane for wastewater treatment, J. Membr. Sci. 488 (2015) 92–102, https://doi.org/10.1016/j.memsci.2015.04.020.
[75] S. Dadari, M. Rahimi, S. Zinadini, Novel antibacterial and antifouling PES nanofiltration membrane incorporated with green synthesized nickel-bentonite nanoparticles for heavy metal ions removal, Chem. Eng. J. 431 (2022) 134116, https://doi.org/10.1016/j.cej.2021.134116.
[76] F. Medhat Bojnourd, M. Pakizeh, Preparation and characterization of a PVA/PSf thin film composite membrane after incorporation of PSSMA into a selective layer and its application for pharmaceutical removal, Sep. Purif. Technol. 192 (2018) 5–14, https://doi.org/10.1016/j.seppur.2017.09.054.
[77] W. Zhang, L. Ding, J. Luo, M.Y. Jaffrin, B. Tang, Membrane fouling in photocatalytic membrane reactors (PMRs) for water and wastewater treatment: a critical review, Chem. Eng. J. 302 (2016) 446–458, https://doi.org/10.1016/j.cej.2016.05.071.
[78] F. Su, C. Lu, J.-H. Tai, Separation of benzene, toluene, ethylbenzene and P-xylene from aqueous solutions by carbon nanotubes/polyvinylidene fluoride nanocomposite membrane, J. Water Resour. Prot. 8(10), Article 10 (2016), https://doi.org/10.4236/jwarp.2016.810075.
[79] H. Sardarabadi, S. Kiani, H. Karkhanechi, S.M. Mousavi, E. Saljoughi, H. Matsuyama, Effect of nanofillers on properties and pervaporation performance of nanocomposite membranes: a review, Membranes 12(12), Article 12 (2022), https://doi.org/10.3390/membranes12121232.
[80] H. Wu, X. Niu, J. Yang, C. Wang, M. Lu, Retentions of bisphenol A and norfloxacin by three different ultrafiltration membranes in regard to drinking water treatment, Chem. Eng. J. 294 (2016) 410–416, https://doi.org/10.1016/j.cej.2016.02.117.
[81] R. Zhang, Y. Liu, M. He, Y. Su, X. Zhao, M. Elimelech, Z. Jiang, Antifouling membranes for sustainable water purification: strategies and mechanisms, Chem. Soc. Rev. 45 (21) (2016) 5888–5924, https://doi.org/10.1039/C5CS00579E.
[82] D. Emadzadeh, T. Matsuura, M. Ghanbari, A.F. Ismail,) Hybrid forward osmosis/ultrafiltration membrane bag for water purification, Desalination 468 (2019) 114071, https://doi.org/10.1016/j.desal.2019.114071.